8-2004

Embrittlement and Localized Corrosion in Alloy HT-9

Sudheer Sama
University of Nevada, Las Vegas

EMBRITTLEMENT AND LOCALIZED CORROSION IN ALLOY HT-9

by

Sudheer Sama

Bachelor of Technology in Mechanical Engineering
Gulbarga University, India
December 2000

A thesis submitted in partial fulfillment
of the requirements for the

Master of Science Degree in Mechanical Engineering
Department of Mechanical Engineering
Howard R. Hughes College of Engineering

Graduate College
University of Nevada, Las Vegas
August 2004

UNLV
UNIVERSITY OF NEVADA, LAS VEGAS

Thesis Approval

The Graduate College
University of Nevada, Las Vegas

August 6, , 2004

The Thesis prepared by

Sudheer Sama

Entitled

Embrittlement and Localized Corrosion in Alloy HT-9.

is approved in partial fulfillment of the requirements for the degree of

Master of Science in Mechanical Engineering.

[redacted]
Examination Committee Chair

[redacted]
Dean of the Graduate College

[redacted]
Examination Committee Member

[redacted]
Examination Committee Member

[redacted]
Graduate College Faculty Representative

1017-53

ABSTRACT

Embrittlement and Localized Corrosion in Alloy HT-9

By

Sudheer Sama

Dr. Ajit K.Roy, Examination Committee chair
Associate Professor of Mechanical Engineering
University of Nevada, Las Vegas

This investigation is focused on the evaluation of stress corrosion cracking (SCC), hydrogen embrittlement (HE) and localized corrosion susceptibility of Alloy HT-9 in neutral and acidic solutions at 30, 60 and 90°C. Constant-load and slow-strain-rate (SSR) testing techniques were used to evaluate the SCC and HE behavior of this alloy by using smooth and notched tensile specimens. Hydrogen effect on the cracking behavior was evaluated by applying cathodic (negative) potential to the test specimens. Localized corrosion susceptibility was evaluated by cyclic potentiodynamic polarization technique. The results of constant load SCC testing showed a threshold stress at 80% of the material's yield strength value in the 90°C acidic solution. Reduced ductility and true failure stress were observed in the SSR tests due to the combined effect of acidic pH and increased temperature. SCC testing under cathodic charging showed further reduction in ductility and true failure stress. Polarized specimens showed pitting in the acidic solution. Fractographic evaluations by scanning electron microscopy revealed ductile and brittle failures, respectively in the neutral and acidic environments.

TABLE OF CONTENTS

LIST OF TABLES

LIST OF FIGURES

ACKNOWLEDGEMENTS

I would like to acknowledge the immense assistance and support provided by Dr. Ajit K. Roy, the Principal Investigator in this project from the inception of this task.

I would like to thank Dr. Anthony Hechanova, Dr. Brendan J O'Toole, and Dr. Satish Bhatnagar for their direct and indirect contribution throughout this investigation.

I would like to acknowledge the help provided by my coworkers in this project.

Finally I would like to thank the U.S. Department of Energy for financial support of this project.

CHAPTER 1

INTRODUCTION

Nuclear waste consists of used fuel released from nuclear reactors. In the United States, the existing nuclear reactors are expected to produce approximately 150,000 metric tons of spent fuel over their life times. Almost 50 percent (%) of this wastage is designed to be stored in a geological repository at the Yucca Mountain site near Las Vegas, Nevada. It has been estimated that by 2050 there may be 1 million tons of discharged fuel worldwide. This projection may indicate a necessity of constructing and commissioning an additional repository of the scale of Yucca Mountain somewhere in the world for every three to four years.

The detrimental effect of SNF is accountable is attributable only to 1% of its content. This 1% is primarily made up of plutonium, neptunium, americium, and curium (called transuranic elements) and long-lived isotopes of iodine and technetium created as products from the fission process in nuclear powered reactors [1]. The separation of the long-lived actinides and fission products from the SNF, and transmuting them into short-lived actinides or non-radioactive waste would ease the constraints for geologic repositories, reduce their building costs, and increase the public acceptance. For this reason, accelerator-driven systems with their transmutation potential are currently being considered as an alternative approach for the nuclear waste management, compared to that associated with the direct disposal of SNF in a geological repository.

The basic process of accelerator-driven nuclear systems is nuclear transmutation that can minimize the inflexible performance requirements of a geological repository by reducing the isolation period for HLW/SNF from 10,000 years to much shorter duration and can also eliminate the need for another geologic repository. In essence, the benefits drawn from transmuting of nuclear waste components are: the reduction of long-lived nuclear contents, the elimination of a future geological repository and the partitioning and transmutation process allows for the use of optimized waste forms that can be highly resistant to leaching and other natural processes [2].

Transmutation refers to the minimization or elimination of long-lived actinides and fission products from spent fuels discharged from operating nuclear reactors. An important component of the transmutation facility is a subcritical-target, which produces an intense neutron flux by impingement of accelerator proton beam onto it by a process known as spallation.

A large amount of heat can be generated in the target material that will be contained in a sub-system structural container. Molten lead-bismuth-eutectic (LBE) has been identified as a spallation target to produce neutrons by the incident proton beams, and at the same time acting as a coolant, thus removing the generated heat. During this process, the target structural material may experience plastic or mechanical deformation because of the thrust produced by the bombardment of the high-speed protons onto the molten LBE.

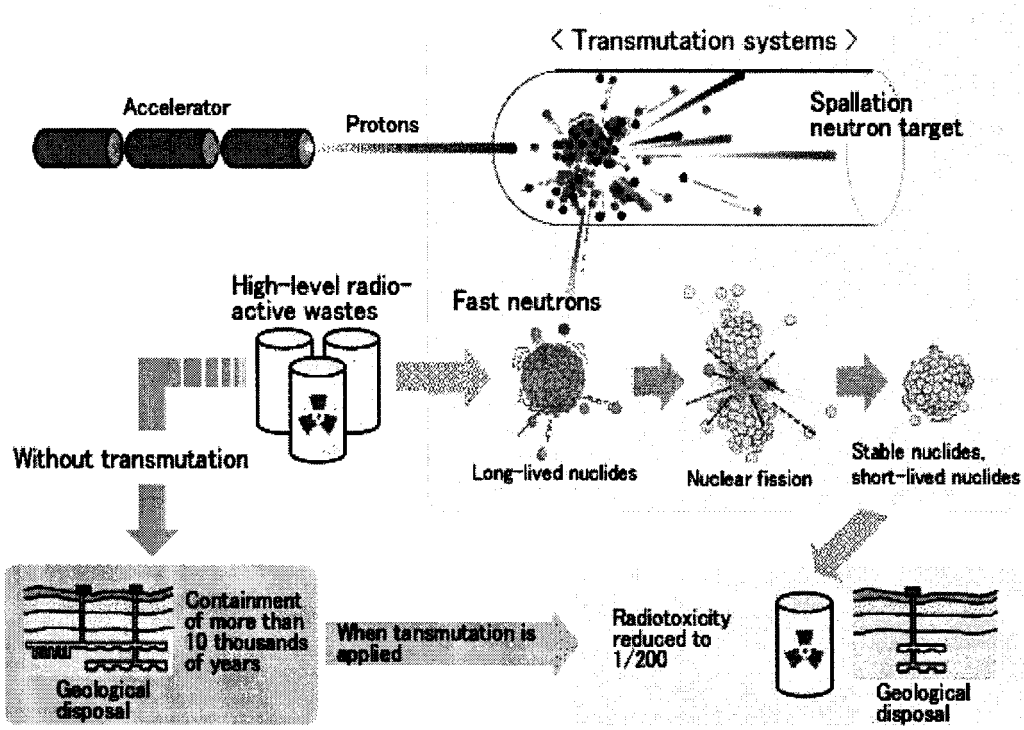

Figure 1.1 Schematic Illustration of Accelerator Driven Transmutation Process

Temperature ranging from 400 to 600°C can be developed in the molten LBE during this process. In addition, the LBE-containing structural material may undergo environment assisted degradation and high temperature deformation [3]. The environments associated with the target systems can have an appreciable amount of hydrogen and helium that can induce degradations such as stress corrosion cracking (SCC), hydrogen embrittlement (HE), and localized corrosion [4]. Hydrogen and helium generation are the result of neutron formation during the transmutation process.

SCC is an environment-assisted cracking of an alloy resulting from the combined effect of a corrosive environment and a tensile stress. The stress may result from applied forces or locked-in residual stresses. Only specific combinations of alloy and chemical environment can lead to SCC. Usually, SCC begins with the rupturing of the protective

oxide film on the metal surface by either mechanical means or by the action of chemical species, such as chloride ion. The cracks resulting from SCC may be either ductile or brittle in nature or a combination of both. Cracking may be intergranular, transgranular, or mixed mode depending on the alloy, its microstructure, and the environment. As stated earlier, hydrogen and helium produced during nuclear reactions can segregate to vacancy clusters and internal voids, thus eventually leading to HE in the target structural material [5].

The HE process may depend on two major factors: (1) the origin of the hydrogen; (2) the transport processes involved in moving the hydrogen from its source to the locations where it reacts with the metal to cause embrittlement. Body-centered cubic (bcc) metals are the most susceptible to HE [6]. The Primary characteristics of HE are its strain-rate sensitivity, its temperature dependence and its susceptibility to delayed fracture. Localized corrosion is a degradation mode in which an intense attack takes place at localized sites on the surface of the material while the rest corrodes at a lower rate.

This investigation is focused on the evaluation of SCC and HE of Alloy HT-9, a leading candidate target structural material, in aqueous environments of two different pH values using constant-load (CL) and slow-strain-rate (SSR) testing techniques. The use of the SSR and CL testing methods was based on their simplicity in performing the desired testing. The SSR testing is based upon a principle by which a test specimen is pulled in tension until fracture under a very slow strain rate condition to optimize combined effect of environment and mechanical constraint. Further, electrochemical studies were performed to evaluate the susceptibility of Alloy HT-9 to localized corrosion including pitting and crevice corrosion in similar environments. In addition, the metallographic and

fractographic evaluations of the broken specimens were performed by optical microscopy and scanning electron microscopy (SEM), respectively.

In essence, this thesis presents the results of SCC, HE and localized corrosion studies of Alloy HT-9 in aqueous environments that may constitute significant baseline information on the performance of this alloy as a function of different environmental and mechanical parameters including temperature, pH, and hydrogen ion (H^+) concentration and loading mode. It should, however, be noted that a direct comparison of the performance of this material in molten LBE to that in the aqueous environments is not possible since the degradation in the former case is the result of liquid-metal embrittlement that does not involve ionic transfer but experience reduction in cohesive strength among surface atoms due to their reactions with the molten metal. Space evaluation of the SCC and localized corrosion susceptibility in the molten LBE is currently being pursued at the Los Alamos National Laboratory (LANL). Further, an infrastructure development to perform LBE experiments at UNLV is in progress.

.

CHAPTER 2

MATERIAL AND ENVIRONMENTS

2.1. Test Material

The martensitic stainless steels are currently finding extensive application in nuclear reactors as substitutes for austenitic steels [7]. They are basically alloys of carbon (C) and chromium (Cr) having body-centered-cubic (bcc) or body-centered tetragonal (bct) martensitic crystal structure in the hardened state. They are ferromagnetic and hardenable by heat-treatments. Martensitic stainless steels are usually preferred for their relatively high strength, moderate resistance to corrosion and good fatigue properties following suitable thermal treatments. The Cr content of these materials normally ranges between 9 to 18 wt%, and their C content can be as high as 1.2 wt%. The composition of Cr and C are balanced to ensure a martensitic structure after hardening. Molybdenum (Mo) and nickel (Ni) can also be added to improve the mechanical properties or the corrosion resistance. When higher Cr levels are used to improve corrosion resistance, the presence of Ni can also help in maintaining the desired microstructure and preventing the formation of excessive free-ferrite [8].

Since the as-hardened martensitic structure is quite brittle, this material is typically reheated at lower temperatures to relieve the internal stresses within the microstructure or reheated to slightly higher temperatures to soften (temper) the material to intermediate

hardness levels. Two martensitic alloys are of great interest in the United States. They are: Alloy HT-9 and T-91, both of which contain Cr and Mo. These alloys have been extensively used in Europe and USA as target structural materials in the transmutation systems as well as for the internal components in the U.S experimental liquid metal fast breeder reactors (LMFBR) due to their moderate corrosion resistance, optimum strength and the ease of manufacturing as well as their relatively lower cost [9]. Alloy HT-9 is a Swedish nuclear grade martensitic iron-nickel-chromium-molybdenum (Fe-Ni-Cr-Mo) stainless steel. T-91 falls within an ASTM designation [10] having Cr, Mo, Nb and V in it.

Alloy HT-9 was specifically developed for high temperature applications where the corrosion-resistance inherent in austenitic stainless steels is not required. It has good swelling resistance and is also resistant to irradiation embrittlement particularly at 60°C [11]. It has been an excellent material for cladding and duct applications in liquid-metal reactors. The thermal/physical properties and history of development of Alloy HT-9 are shown in Tables 2.1 and 2.2, respectively [12, 13].

Table 2.1 Thermal and Physical Properties of Alloy HT-9

Property	Alloy HT-9
Thermal Conductivity, W/m*K	28
Modulus of Elasticity, GPa (10^6 psi)	160
Poisson's Ratio	0.33
Coefficient of Thermal Expansion per °C (°F) * 10^{-6}	12.5

Table 2.2 History and Properties of Alloy HT-9

Alloy	Application History	Properties
HT-9	• Structural applications in super critical fossil power plants	• Lower coefficient of thermal expansion and high thermal conductivity than austenitic steels • High swelling resistance in fast neutron, ion and electron irradiation conditions • High creep strength • Higher Cr corrosion rates than austenitic/Ni based alloys • Addition of Cu may cause irradiation embrittlement

The chemical composition and ambient temperature mechanical properties of Alloy HT-9 tested in this study are given in Tables 2.3 and 2.4, respectively.

Table 2.3 Chemical Composition of Alloy HT-9 Tested

Material/ Heat #	Elements (wt%)													
	C	Mn	P	S	Si	Cr	Ni	Mo	Cu	V	W	Cb	B	Ce
Alloy HT-9 /2048	0.18	0.4	0.012	0.2	0.20	12.26	0.49	1	0.01	0.3	0.46	--	--	--

Table 2.4 Ambient Temperature Mechanical Properties of Alloy HT-9

Material/Heat No.	Yield Strength (ksi)	Ultimate Strength (ksi)	%El	%RA
Alloy HT-9/2048	118	139	22.1	62.3

2.2. Test specimens

An experimental heat of Alloy HT-9 was custom-melted by vacuum induction melting practice at the Timken Research Laboratory followed by fabrication processes to develop round bars. These bars were then austenitized at 1850°F for an hour, followed by an oil-quench. The quenched bars were then tempered at 1150°F for 1.25 hour and were subsequently air-cooled. The purpose of quenching and tempering was to achieve a fully tempered martensitic microstructure with a bcc structure without any retained austenite.

Cylindrical smooth specimens of 4-inch total length; 1-inch gage length and 0.25-inch gage diameter were machined from these heat-treated bars in the longitudinal rolling direction. Some of these cylindrical tensile specimens were notched at the gage section by machining a V-shaped notch having an angle of 60° and a 0.05-inch depth around the diameter (0.156-inch) at the middle of the gage section. The stress concentration factor (K_t) corresponding to this notch was roughly about 2.9. The magnitude of K_t [14] was determined from the following calculation by using the plot shown in Figure 2.1.

$$\frac{D}{d} = \frac{0.250\,in}{0.156\,in} \qquad \text{(Equation 3.1)}$$

$$\frac{D}{d} = 1.60$$

$$\frac{r}{d} = \frac{0.005\ in}{0.156\ in}$$

$$\frac{r}{d} = 0.032 \qquad \text{(Equation 3.2)}$$

Where,

D = gage diameter,
d = notch diameter
r = radius of curvature at the root of the notch

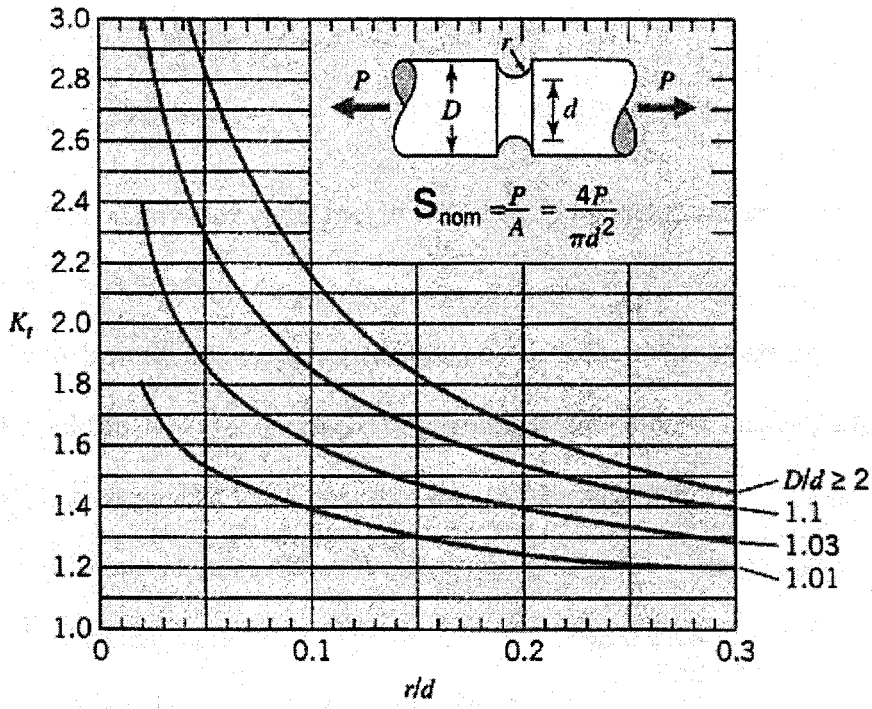

Figure 2.1 Stress Concentration Factors for Grooved Shafts

According to the ASTM designation E 8 [15], the aspect ratio of both smooth and notch specimens was maintained at 4. Specimens used in electrochemical polarization experiments were machined according to ASTM designation G 5 [16]. The schematic views of the smooth, notched and polarization specimens are shown in Figures 2.1, 2.2 and 2.3, respectively.

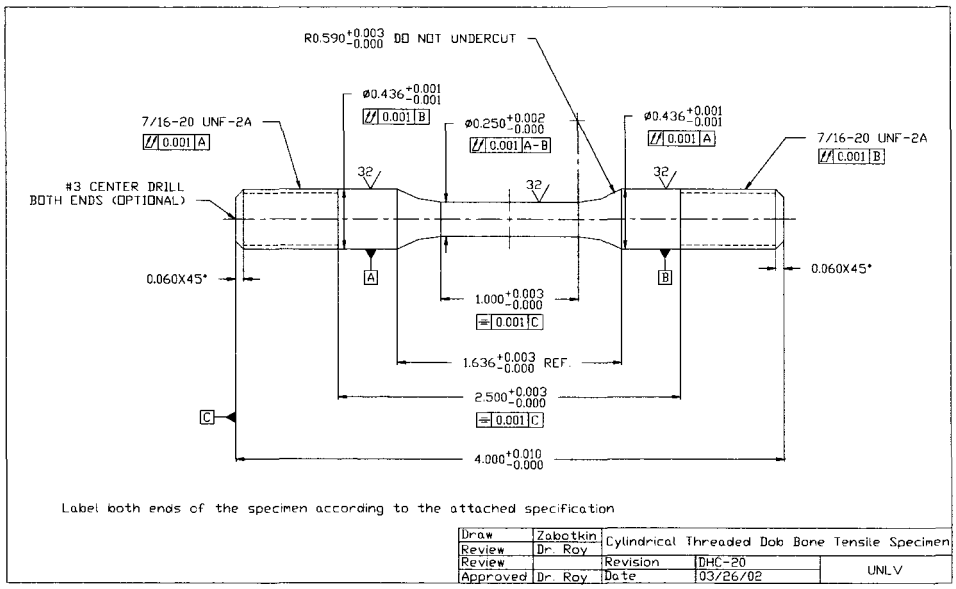

Figure 2.2 Schematic View of Smooth Tensile Specimen

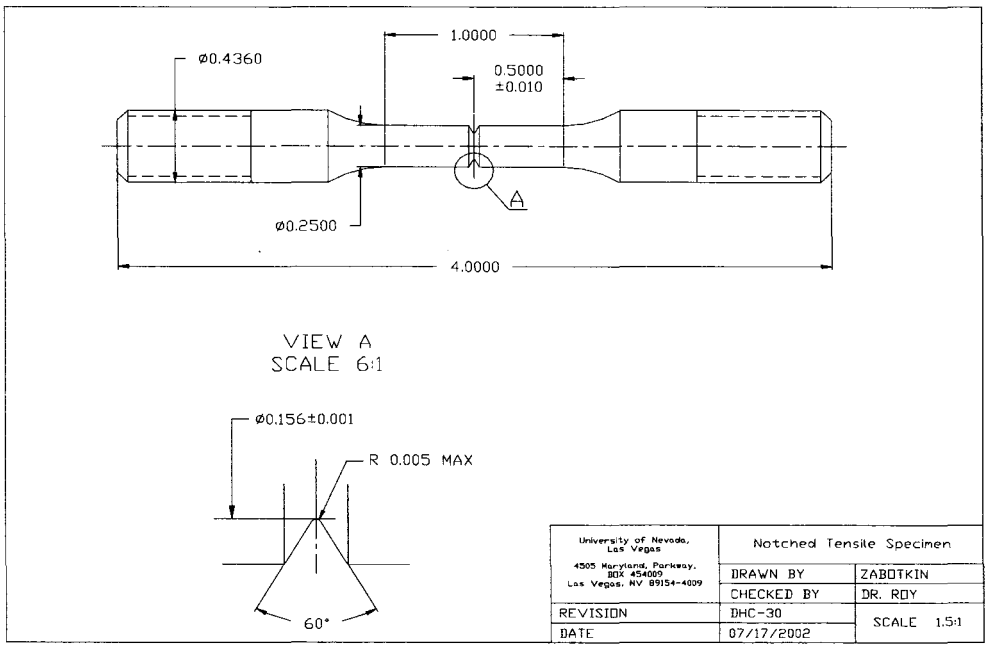

Figure 2.3 Schematic View of Notch Tensile Specimen

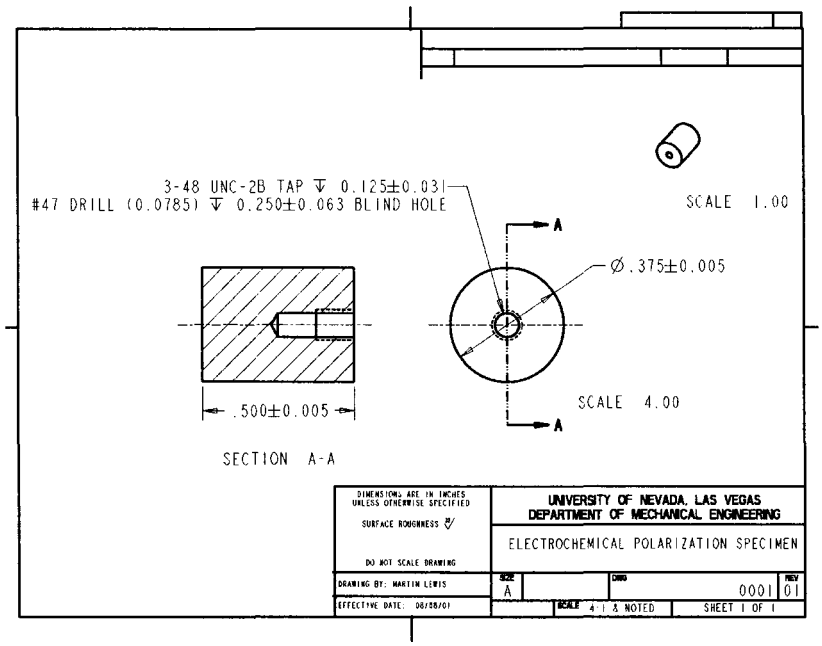

Figure 2.4 Schematic View of Polarization Specimen

2.3. Test Environments

As mentioned earlier, the performance of Alloy HT-9 needs evaluation in the presence of molten LBE. The susceptibility of Alloy HT-9 using self-loaded specimens (C-ring/U-bend) is to be studied soon at LANL/UNLV using a LBE testing facility. Since, the materials performance laboratory (MPL) at UNLV has no capability to conduct SCC experiments in the presence of molten LBE, corrosion studies have been performed at MPL in the presence of aqueous environments using different state-of-the-art testing techniques. These environments include neutral solution with pH ranging between 6 and 6.5, and acidic solution with pH ranging from 2 to 2.5, as shown in Table 2.5. The susceptibility of Alloy HT-9 to SCC, HE and localized attack was evaluated in these environments at 30, 60 and 90°C.

Table 2.5 Chemical Composition of Test Solutions (grams/liter)

Environment (pH)	$CaCl_2$	K_2SO_4	$MgSO_4$	NaCl	$NaNO_3$	Na_2SO_4
Neutral (6-6.5)	2.769	7.577	4.951	39.973	31.529	56.742
Acidic (2-2.5)	Same as above except for an addition of HCl to attain for the desired pH range					

CHAPTER 3

EXPERIMENTAL PROCEDURES

The susceptibility of Alloy HT-9 to SCC in acidic and neutral environments was evaluated by using both constant-load (CL) and slow-strain-rate (SSR) testing techniques at temperatures ranging from ambient to 90°C. The susceptibility of this alloy to localized corrosion was evaluated by using electrochemical cyclic potentiodynamic polarization (CPP) technique. The effect of hydrogen on the cracking behavior of this alloy was determined by applying cathodic (negative) electrochemical potential while the specimen was strained in tension in an aqueous solution. Further, optical microscopy and SEM were used to evaluate the metallurgical microstructures and the morphology of failure in the tested specimens, respectively.

3.1. Constant-load Testing

A calibrated proof ring was used for constant-load (CL) testing. Proof rings were specifically-designed to meet the National Association of Corrosion Engineers (NACE) standards [17]. Each individually calibrated proof ring was made by Cortest Inc and was accompanied by a calibration curve showing the load versus deflection of this ring. Test specimens were loaded under a stress state of uniaxial tension. Ring deflection was measured with a 8-9" diameter micrometer, with the supplied dial indicator providing a

check. These poof rings were fabricated from precision-machined alloy steel. Tension on the proof ring was quickly and easily adjusted using a standard wrench on the tension-adjusting screw and lock nut. A thrust bearing distributed the load and prevented seizure. Specimen grips in these proof rings were made of stainless steel, fully-resistant to the testing environments. The environmental test chamber was secured by O-ring seals that prevented any leakage during testing. The environmental chambers made of highly corrosion-resistant Hasteloy C-276 were used for testing at elevated temperatures. The experimental setup is shown in Figure 3.1.

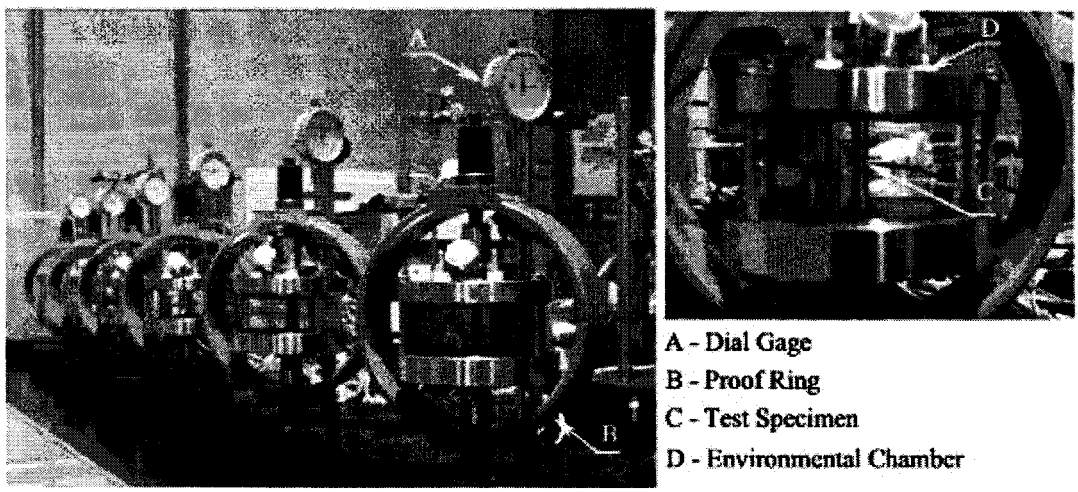

Figure 3.1 Constant-load Test Setup

The amount of deflection needed to apply the desired load in the CL testing was determined by use of the calibration curve of the proof ring, as shown in Figure 3.2. The magnitude of the applied stress was based on the ambient temperature tensile yield strength (YS) of the test materials. Specimens were loaded at stress values equivalent to different percentages of the individual material's YS value, and the corresponding time-

to-failure (TTF) was recorded. The determination of the SCC tendency using this technique was based on the TTF for the maximum test duration of 30 days. An automatic timer attached to the test specimen recorded the TTF. The cracking susceptibility was expressed in terms of a threshold stress (σ_{th}) below which cracking did not occur during the maximum test duration of 30 days.

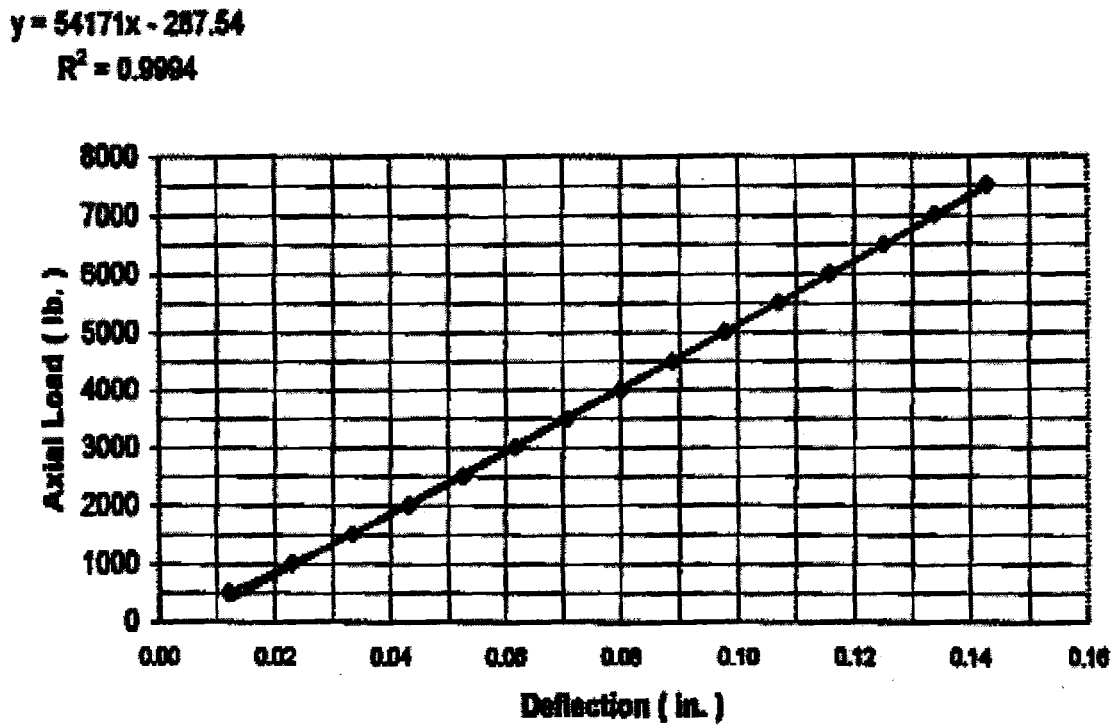

Figure 3.2 A Typical Calibration Curve for a Proof Ring

3.2. Slow-Strain-Rate Testing

Before 1965, only constant-load or constant-strain tests of smooth and notched specimens of various configurations were used to assess the SCC tendency in metals. During the late 1960s, a dynamic SCC evaluation technique had emerged which is known

as constant-strain-rate or slow-strain-rate testing (SSR) technique [17]. SSR testing used in this investigation was performed in a specially-designed system known as a constant-extension-rate-testing (CERT) machine, as shown in Figure 3.3. This equipment allowed testing to simulate a broad range of load, temperature, pressure, strain-rate and environmental conditions using both mechanical and electrochemical corrosion testing techniques. These machines, designed and manufactured by the Cortest Inc, offered accuracy and flexibility in testing the effects of strain rate, providing up to 7500 lbs of load capacity with linear extension rates ranging from 10^{-5} to 10^{-8} in/sec.

To ensure the maximum accuracy in test results, this apparatus was comprised of a heavy-duty load-frame that minimized the system compliance while maintaining precise axial alignment of the load train. An all-gear drive system provided consistent extension rate. This machine provided the maximum flexibility and working space for test sample configuration, environmental chamber design, and accessibility. An added feature included in this model (model# 3451) for ease of operation was a quick-hand wheel to apply a pre-load prior to the operation.

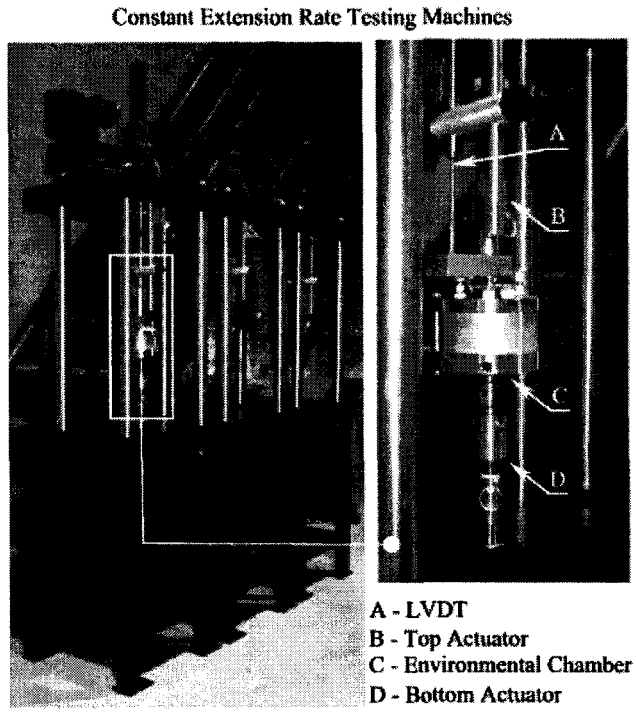

Figure 3.3 CERT Machines for SSR Testing

The SSR test setup used in this study consisted of a top-loaded actuator, testing chamber, linear variable differential transducer (LVDT) and load cell as shown in Figure 3.4. The top-loaded actuator was intended to pull the specimen at a specified strain rate so that the spilled solution, if any, would not damage the actuator. A heating cartridge was connected to the bottom cover of the environmental chamber for elevated-temperature testing. A thermocouple was connected on the top cover of this chamber to monitor the inside temperature. The load cell was intended to measure the applied load through an interface with the front panel user interface. The LVDT was used to record the displacement of the gage section during the SSR testing.

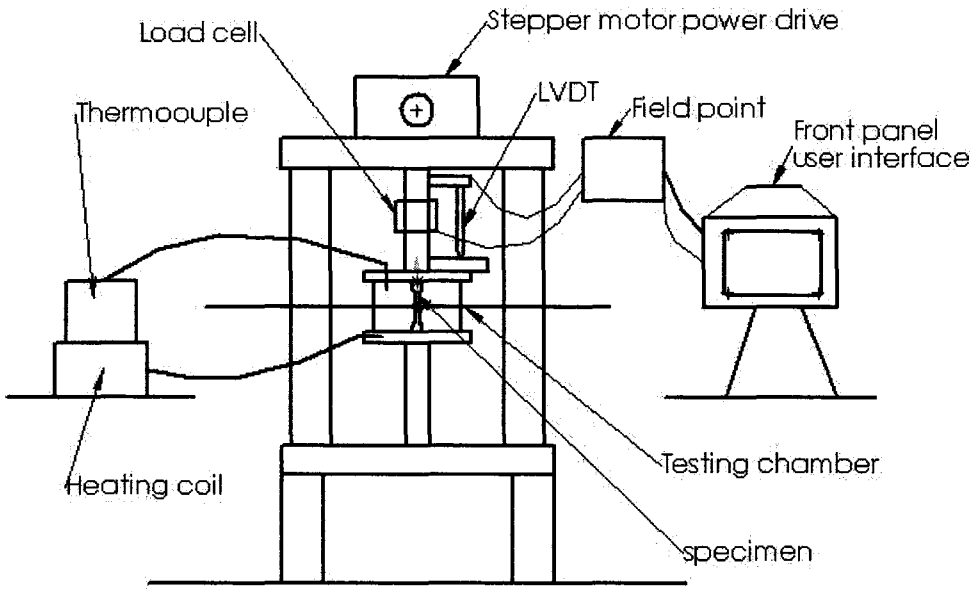

Figure 3.4 SSR Test Setup

Prior to the performance of SCC testing by the SSR technique, the load-frame-compliance factor (LFCF- the deflection in the frame per unit load), was determined by using ferritic type 430 stainless steel. The generated LFCF data are shown in the Figure 3.5. These LFCF values were inputted to a load frame acquisition system prior to the SCC testing. The resultant LFCF values are also shown in Figure 3.5.

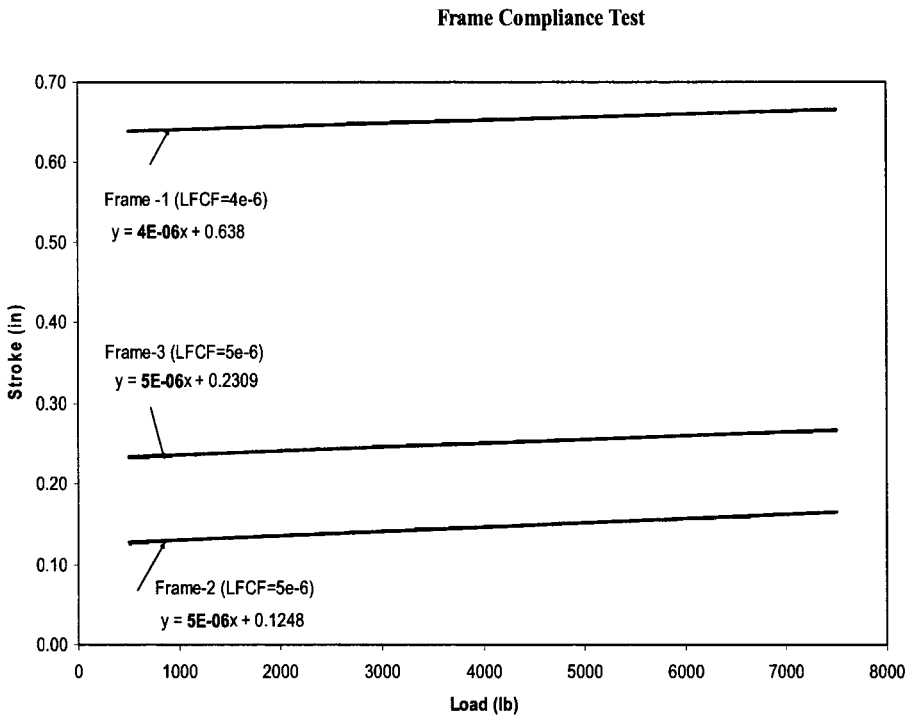

Figure 3.5 Load Frame Compliance Test

A strain rate of $3.3x10^{-6}$ s^{-1} was used during the SSR testing. This strain rate was selected based upon prior research work performed at the Lawrence Livermore National Laboratory (LLNL) [18]. It is well known that the SCC occurrence is an effect of two significant factors such as the applied/residual stress and a susceptible environment. If the stress is applied at a very fast rate to the test specimen, while it is exposed to the aqueous environment, the resultant failure may not be different from the conventional mechanical deformation produced without an environment. On the other hand, if the strain rate is too slow, the resultant failure may simply be attributed to the corrosive damage due to environmental interaction with the material, thus, causing breakdown of the protective surface film. In view of this rationale, the SSR testing at LLNL was initially conducted at strain rates ranging between 10^{-5} and 10^{-7} s^{-1}. Based

upon the experimental work at LLNL, it was determined that a strain rate of around 10^{-6} s^{-1} would provide the most effective contributions of both the mechanical and environmental variables in enhancing the environment-induced cracking susceptibility during the SSR testing.

During SCC testing by the SSR method, the specimen was continuously strained in tension until fracture, in contrast to more conventional SCC test conducted under a sustained loading condition. The application of a slow dynamic straining during the SSR testing to the specimen caused failure that probably might not occur under a constant load or might have taken a prohibitively longer duration to initiate cracks in producing failures in the tested specimens.

Load versus displacement, and stress versus strain curves were plotted during these tests. Dimensions (length and diameter) of the test specimens were measured before and after testing. The cracking tendency in the SSR tests was characterized by the time-to-failure (TTF), and a number of ductility parameters such as the percent elongation (%El) and the percent reduction in area (%RA). Further, the maximum stress (σ_m) and the true failure stress (σ_f) obtained from the stress-strain diagram and the final dimensions were taken into consideration. The magnitudes of %El, %RA, σ_m and σ_f were calculated using the following equations:

$$\% \text{ El} = \left(\frac{L_f - L_o}{L_o}\right) \times 100 \; ; \quad L_f > L_o \qquad \text{(Equation 3.1)}$$

$$\%RA = \left(\frac{A_o - A_f}{A_o}\right) \times 100 \; ; \; Ao > A_f \qquad \text{(Equation 3.2)}$$

$$\sigma_f = \frac{P_f}{A_f} \quad \text{(Equation 3.3)}$$

$$\sigma_m = \frac{P_m}{A_m} \quad \text{(Equation 3.4)}$$

$$A = \frac{\pi \times D^2}{4} \quad \text{(Equation 3.5)}$$

Where,

A_0 = Initial cross sectional area

A_m = Cross sectional area at maximum load

A_f= Final cross sectional area at failure

P_m= Ultimate tensile load

P_f= Failure load

L_o= Initial length

L_f= Final length

3.3. Electrochemical Testing

3.3.1. Cyclic Potentiodynamic Polarization Testing

The susceptibility of Alloy HT-9 to localized (pitting and crevice) corrosion was determined by performing cyclic potentiodynamic polarization (CPP) experiments in acidic and neutral environments using EG&G Model 273A potentiostat. The CPP testing was based on a three-electrode polarization concept, in which the working electrode (specimen) acted as an anode and two graphite electrodes (counter electrodes) acted as

cathodes (Figure 3.7). The reference electrode was made of Ag/AgCl solution contained

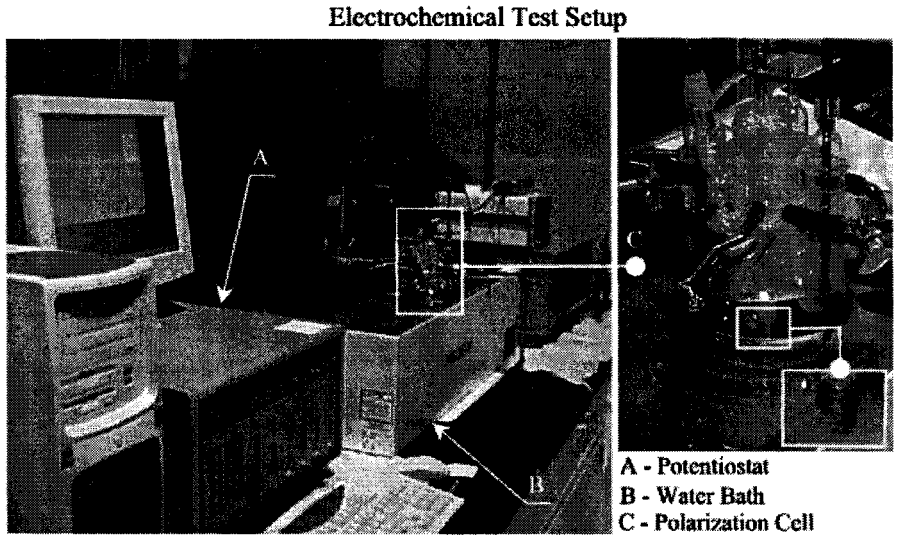

Figure 3.6 Electrochemical Testing Setup

inside a Luggin probe having the test solution that acted as a salt bridge. The tip of the Luggin probe was placed at a distance of 2 to 3 mm from the polarization specimen, as shown in Figure 3.8.

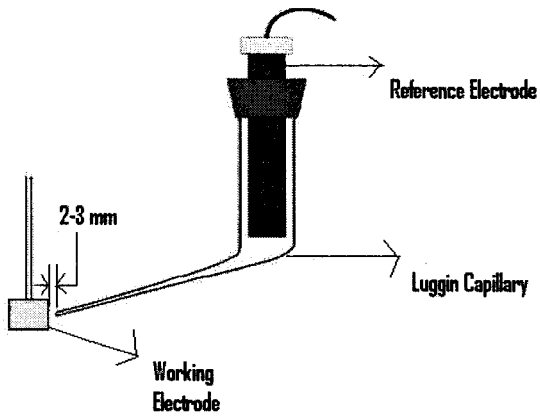

Figure 3.7 Luggin Probe Arrangement

Oxidation reaction takes place at the working electrode (specimen) and reduction reaction occurs at the counter electrodes (graphite rods). At the onset, the corrosion or the open circuit potential (E_{corr}) of the specimen was determined with respect to the Ag/AgCl reference electrode, followed by forward and reverse potential scans at the rate of 0.17 mV/sec. An initial delay of 50 minutes was given to attain a stable E_{corr} value. The magnitudes of the critical pitting potential (E_{pit}) and protection potential (E_{prot}), if any, were determined from the CPP diagram.

Before conducting the CPP test, the potentiostat was calibrated according to the ASTM G 5 Designation. The calibration of this potentiostat was performed to generate a characteristic potentiodynamic polarization curve (Figure 3.9) for ferritic Type 430 stainless steel (SS) in 1N (1 Normal) H_2SO_4 solution at 30°C. Small cylindrical specimens of Type 430 ferritic SS were used to generate the calibration curve. The resultant potentiodynamic polarization curve (Figure 3.10.) was compared to the plot shown in Figure 3.9, taken from the ASTM Designation G 5 [19]. Ideally, the average E_{corr} value for Type 430 ferritic SS in 1N sulphuric acid at 30°C should be approximately - 520 mV with respect to a saturated calomel electrode (SCE).

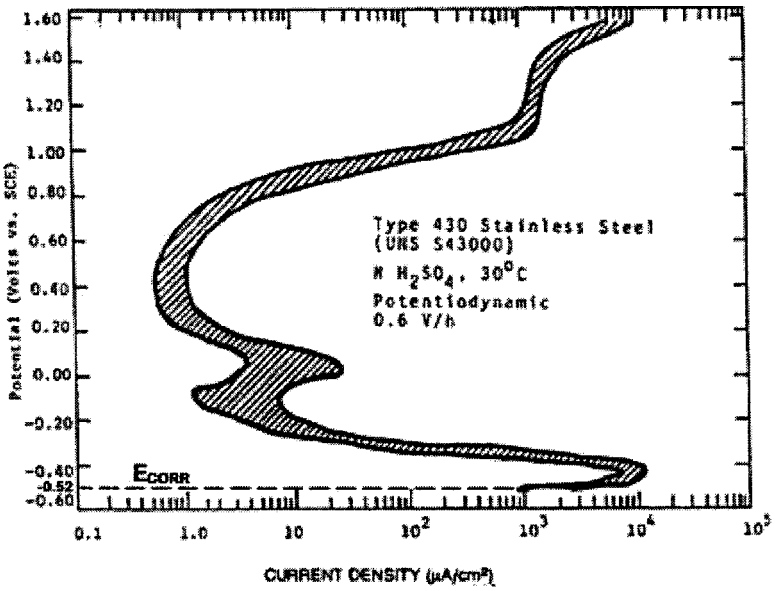

Figure 3.8 Standard Potentiodynamic Polarization Plot (ASTM-G 5)

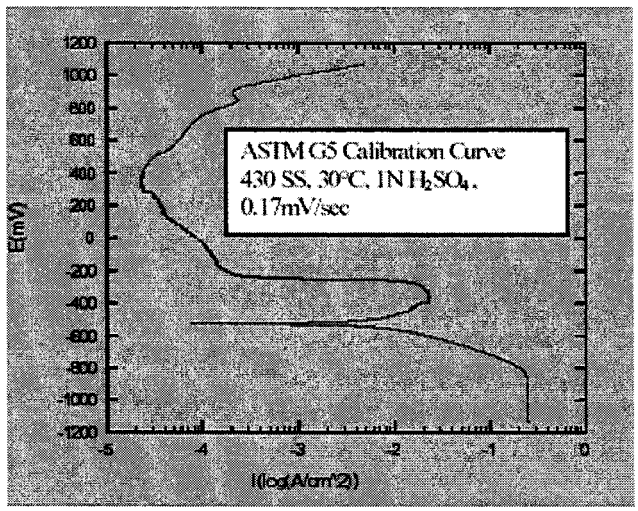

Figure 3.9 Potentiodynamic Polarization Curve for Potentiostat M273A-1

3.3.2. SCC Testing under Potentiostatic Potential

As indicated in the previous section, hydrogen can be generated during the transmutation process due to formation of neutrons. Therefore, attempts were made in

this investigation to evaluate the effect of hydrogen on the cracking susceptibility of Alloy HT-9 while the specimen was strained in tension under the SSR condition. It is a well known that atomic hydrogen can be generated by cathodic polarization ($H^+ + e^- \rightarrow H$) when a metallic material is exposed to an aqueous environment. A cathodic or reduction reaction is associated with the formation of atomic hydrogen (H) that can diffuse into the triaxial stress region within the metal when exposed to a corrosive environment. Accumulation of H in this region can enhance the cracking susceptibility of a stressed material of interest. The susceptibility of an alloy to embrittlement is usually increased in an acidic solution due to the increased concentration of hydrogen ion (H^+) generated during the electrochemical reaction. This phenomenon of degradation is commonly known as hydrogen embrittlement (HE).

The susceptibility of Alloy HT-9 to HE was evaluated by applying cathodic (negative) electrochemical potential (E_{cont}) of –1000 mV with respect to Ag/AgCl reference electrode to the test specimen during straining of the tensile specimen under a similar SSR condition. For SCC testing under E_{cont}, the cylindrical specimens were spot-welded with a conductive metallic wire at their shoulder for electron flow to the gage section of the specimen. The configuration of the spot-welded cylindrical specimen, and the experimental setup under E_{cont} are shown in Figures 3.11 and 3.12, respectively. The specimen was subjected to a selected E_{cont} value for the entire testing duration until it failed. The cracking susceptibility was expressed in terms of ductility parameters (%El and %RA), TTF and σ_f resulting from hydrogen generation due to the cathodic charging.

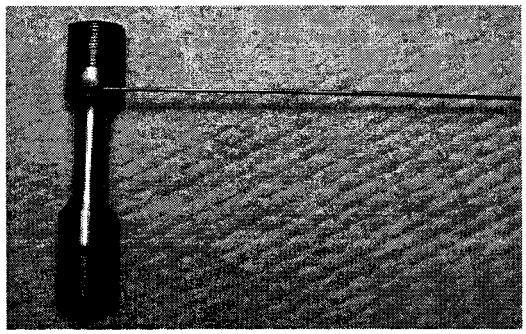

Figure 3.10 Spot-Welded Cylindrical Specimen

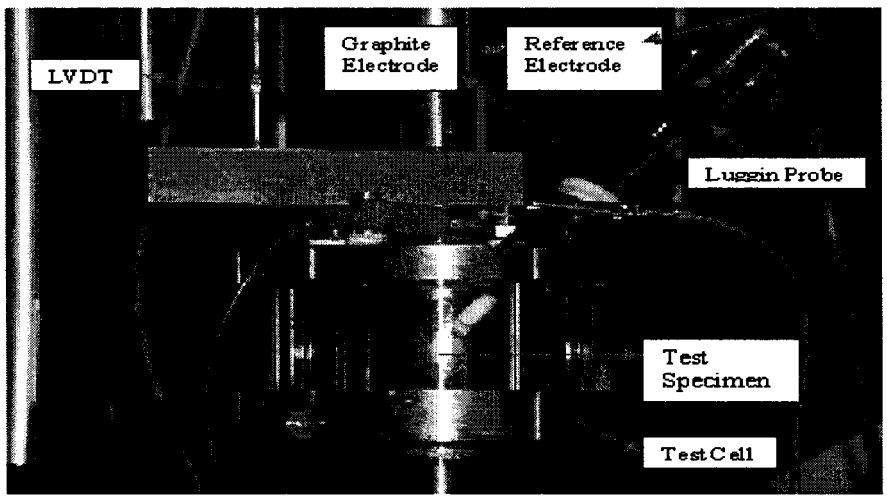

Figure 3.11 HE Test Setup

3.4. Optical Microcopy

Characterization of metallurgical microstructures of engineering materials by optical microscopy is of great importance. Therefore, the tested specimens were sectioned and mounted by a standard metallographic technique, followed by polishing and etching to reveal their microstructures including the grain boundaries. The polished and etched specimens were rinsed in deionized water, and dried with acetone and alcohol prior to their evaluation by a Leica microscope (model # 4001) having a magnification of 1000X.

The presence of secondary cracks, if any, along the gage section of the failed specimen was also determined by this technique.

3.5. Scanning electron microscopy

Failure analyses of metals and alloys involve identification of the types of the failure. Failure can occur by one or more of the several mechanisms, including surface damage, such as corrosion or wear, elastic or plastic deformation and fracture. Failures can be classified as ductile or brittle. The morphology of failure in the tested specimen was determined by scanning electron microscopy (SEM). A Joel SEM (model# 2605) was used to evaluate the fractography of all tested specimen. Energy Dispersive Spectrometry (EDS), interfaced with this SEM, was also used for elemental analysis in the vicinity of the resultant failures.

CHAPTER 4

RESULTS

4.1. Slow- Strain-Rate Tests

4.1.1. Smooth Specimen without E_{cont}

The stress-strain diagrams of Alloy HT-9 obtained in the neutral solution at 30 and 90°C and in the acidic solution at 30, 60 and 90°C are superimposed in Figures 4.1 and 4.2, respectively for comparison purpose. An examination of both figures clearly indicates that the magnitude of strain was gradually reduced with increasing temperature, irrespective of the testing environment. However, the extent of reduction was more pronounced in the acidic solution (Figure 4.2), as expected.

The stress-strain diagrams obtained in the SSR testing and the specimen dimensions before and after testing were used to calculate the ductility parameters (%El and %RA) and the true failure stress (σ_f). The magnitudes of these parameters, and the failure load (P_f) and time-to-failure (TTF) are shown in Table 4.1 as a function of testing environment and temperature. These data reveals that the magnitude of ductility parameters, σ_f and TTF were gradually reduced with increasing temperature, once again showing more pronounced effect in the acidic environment.

The data shown in Table 4.1 are reproduced in a graphical format in Figures 4.3 through 4.6, showing the effects of pH and temperature on %El, %RA, σ_f and TTF. There is a clear indication that all four parameters gradually become reduced with increasing

temperature. These reductions were more pronounced in the acidic solution, as anticipated. It should be noted that all the SSR tests were replicated twice.

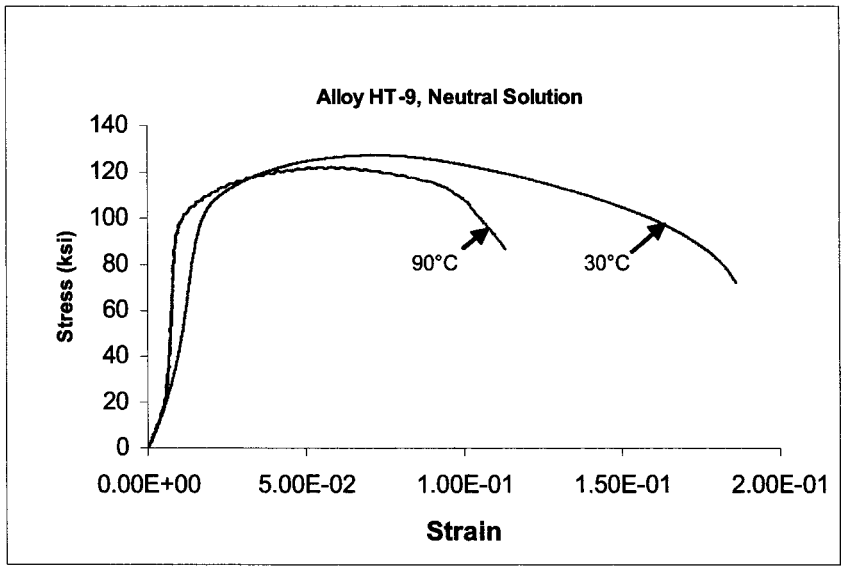

Figure 4.1 Comparisons of Stress-Strain Diagrams

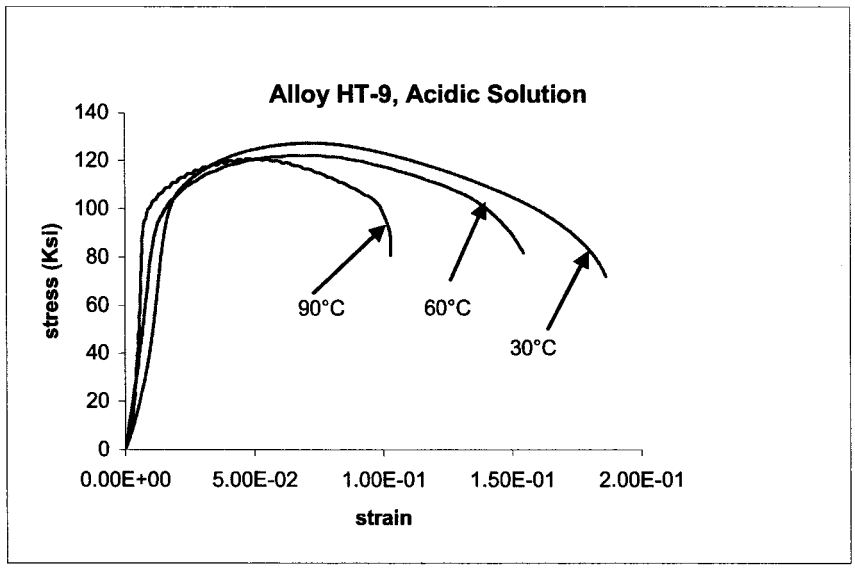

Figure 4.2 Comparisons of Stress-Strain Diagrams

Table 4.1 SSR Test Results using Smooth Specimens

Material/ Heat Number/ Specimen ID	Env	Temp (°C)	%El	%RA	P_f (lbs)	σ_f (Ksi)	TTF (Hour)
HT9/2048/ A19	Neutral	30°C	19.3	61.6	3689.61	191.65	19
HT9/2048/A21	Neutral	30°C	18.86	62.86	3725.79	199.3	18.98
HT9/2048/A33	Neutral	60 °C	18.86	52.32	3959.9	176.8	18.51
HT9/2048/A34	Neutral	60 °C	17.8	51.2	3975.20	175.3	18.52
HT9/2048/A20	Neutral	90°C	13.4	41.7	4248.85	144.5	12.51
HT9/2048/A29	Neutral	90°C	12.4	37.4	4257.3	122.9	12.73
HT9/2048/A8	Acidic	30°C	19.12	55.96	3534.69	171.6	17.93
HT9/2048/A11	Acidic	30°C	18.4	55.72	3575.25	174.45	17.95
HT9/2048/A37	Acidic	60 °C	14.62	48.02	4012.53	154.6	14.9
HT9/2048/A37	Acidic	60 °C	14.8	49.6	4001.32	159.4	14.2
HT9/2048/A38	Acidic	60 °C	14.34	47.92	3755.5	146.98	14.56
HT9/2048/A17	Acidic	90°C	11.02	38.4	3959.3	126.20	12.33
HT9/2048/A18	Acidic	90°C	10.15	35.53	4002.1	117.63	11.9

Temp: Temperature

Env : Environment

P_f : Failure Load

%El : Percentage Elongation

σ_f : True Failure Stress

%RA: Percentage Reduction in Area

TTF: Time-To-Failure

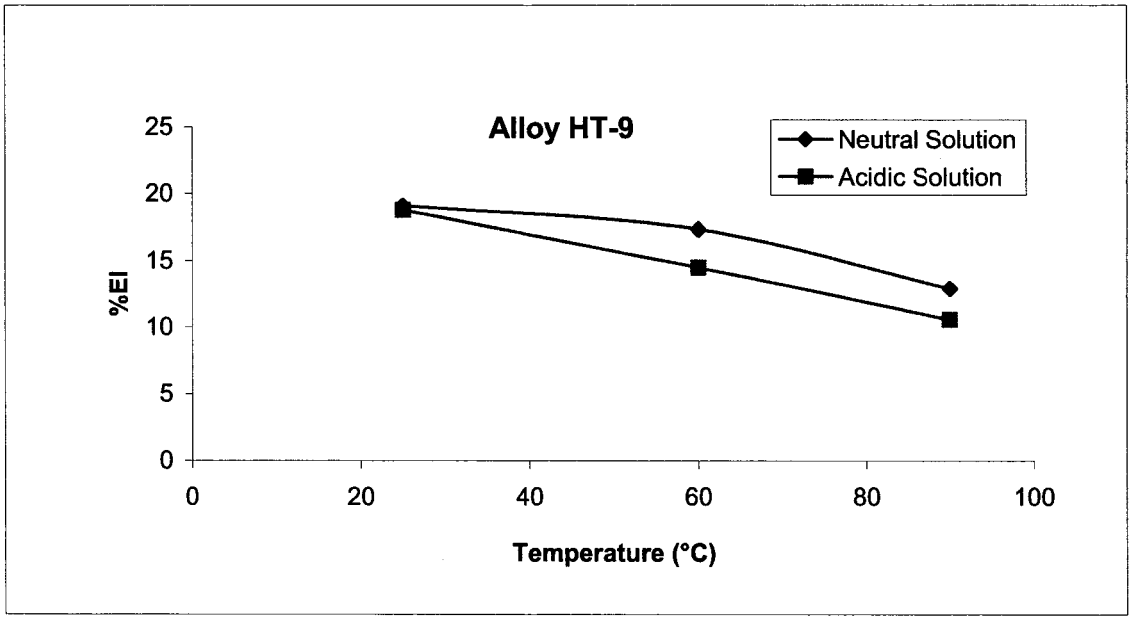

Figure 4.3 Effect of pH and Temperature on %El

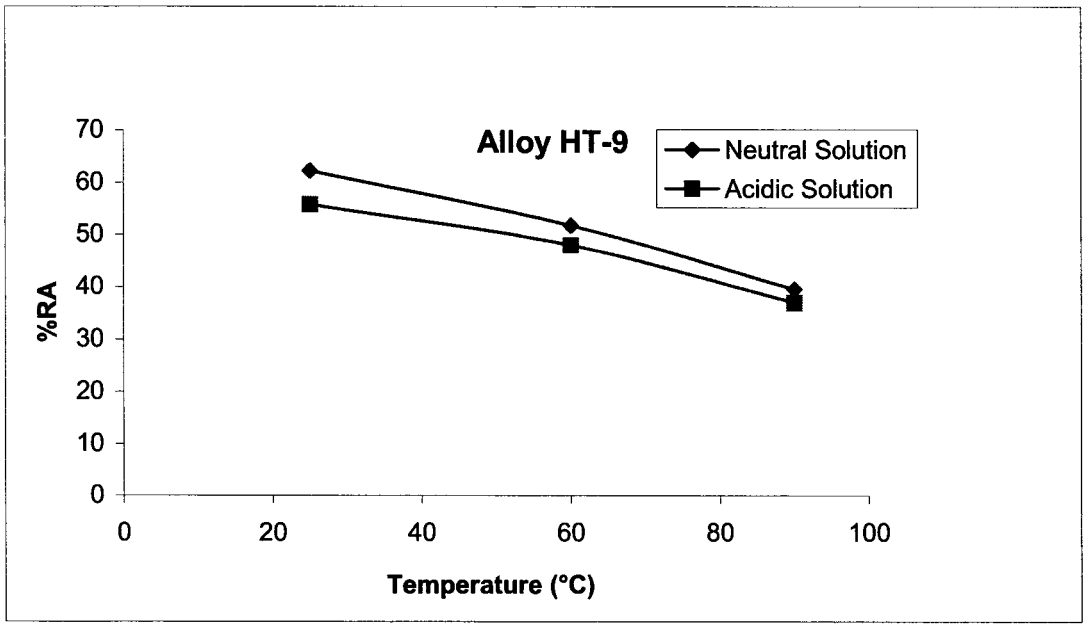

Figure 4.4 Effect of pH and Temperature on %RA

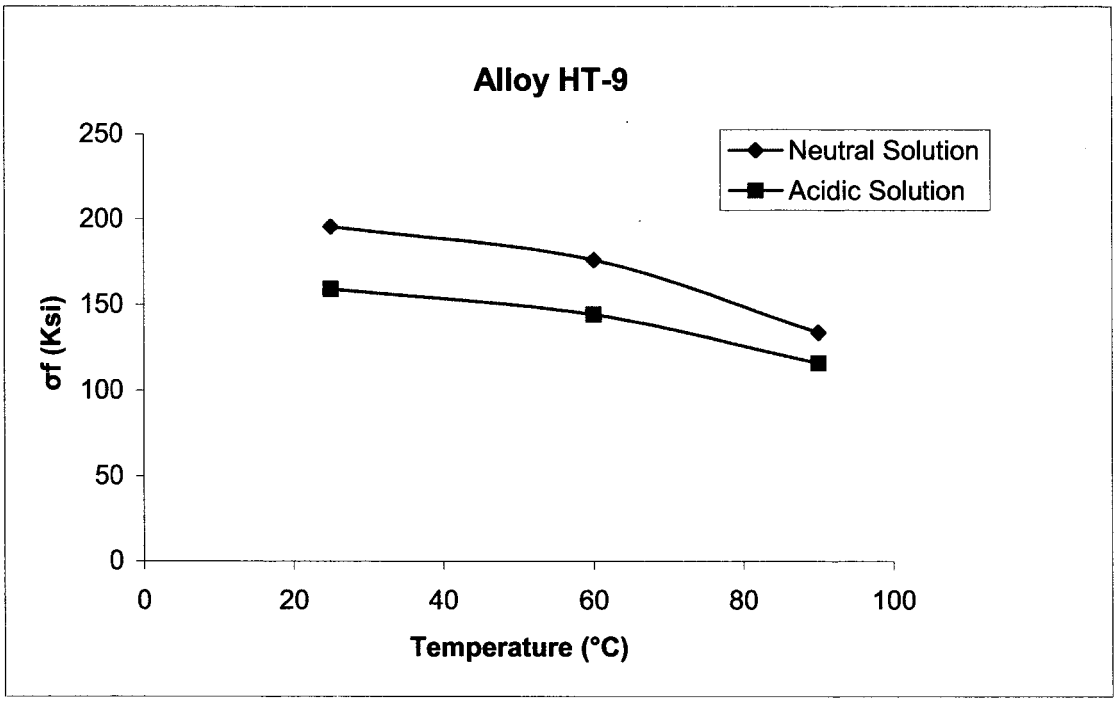

Figure 4.5 Effect of pH and Temperature on σ_f

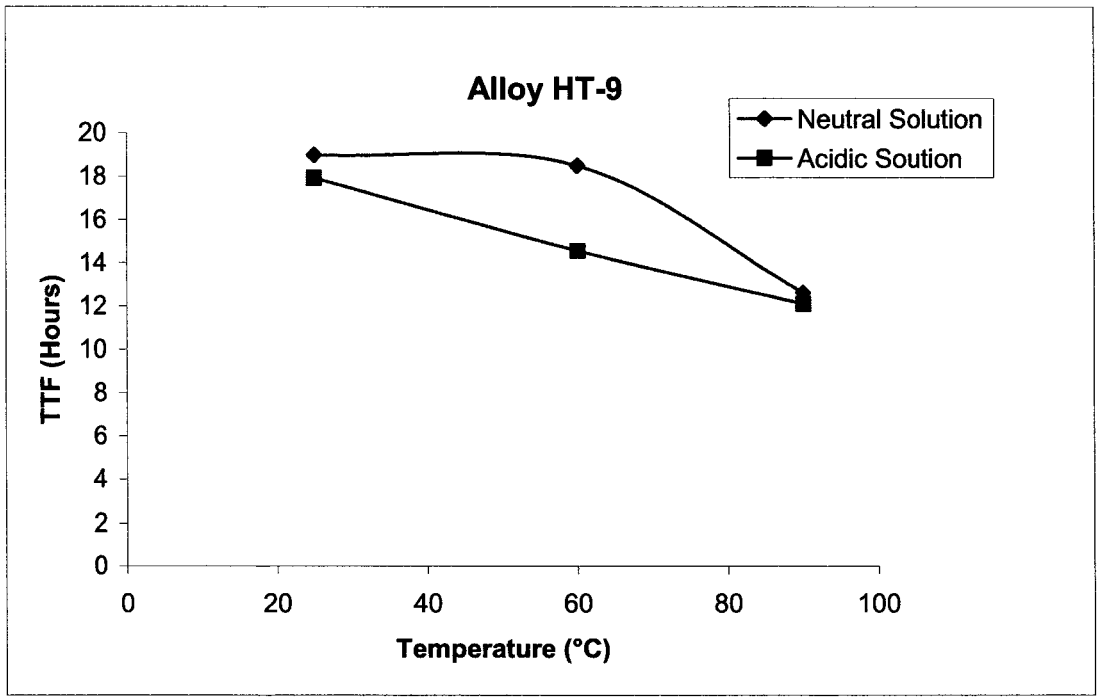

Figure 4.6 Effect of pH and Temperature on TTF

4.1.2. Notched Specimen

A comparison of stress-strain diagram for Alloy HT-9 obtained in air using an MTS unit at ambient temperature involving smooth and notched cylindrical specimens is shown in Figure 4.7. It is obvious from this figure that the presence of a notch in the test specimens reduced the magnitude of the yield strength (YS), ultimate tensile strength (UTS), and the failure stress when tested in air. The effect of pH on the stress-strain diagrams obtained in the 30°C neutral and acidic solutions using notched specimen in the SSR testing is shown in Figure 4.8. These data indicate that the magnitude of the failure strain was substantially reduced in the acidic solution at a comparable testing temperature.

The overall SSR testing data using notched specimens of Alloy HT-9 are given in Table 4.2, showing ductility parameters, failure load, σ_f and TTF as functions of testing environment and temperature. Data shown in Table 4.1 and 4.2 are reproduced in Figures 4.9-4.12 showing the effects of temperature, pH and notch on σ_f, %El, %RA and TTF. These data indicate that the ductility in terms of %RA was reduced in the acidic solution at the elevated temperature due to the presence of notch. However, very little reduction was observed with %El and TTF in either environment due to a change in temperature.

The magnitude of the true failure stress (σ_f) was increased in the presence of a notch due to the reduced cross sectional area at the root of this notch. However, it should be noted that the magnitude of σ_f reduced in the 90°C acidic solution, possibly due to the combined effect of pH and temperature on this parameter. In general, the notched specimen showed significantly reduced %El, %RA, TTF values compared to those obtained with smooth specimens, as expected. The effects of testing temperature and

environment on the maximum load (P_m) and failure load (P_f) are shown in Table 4.3, showing lower values in the acidic solution at the elevated temperature.

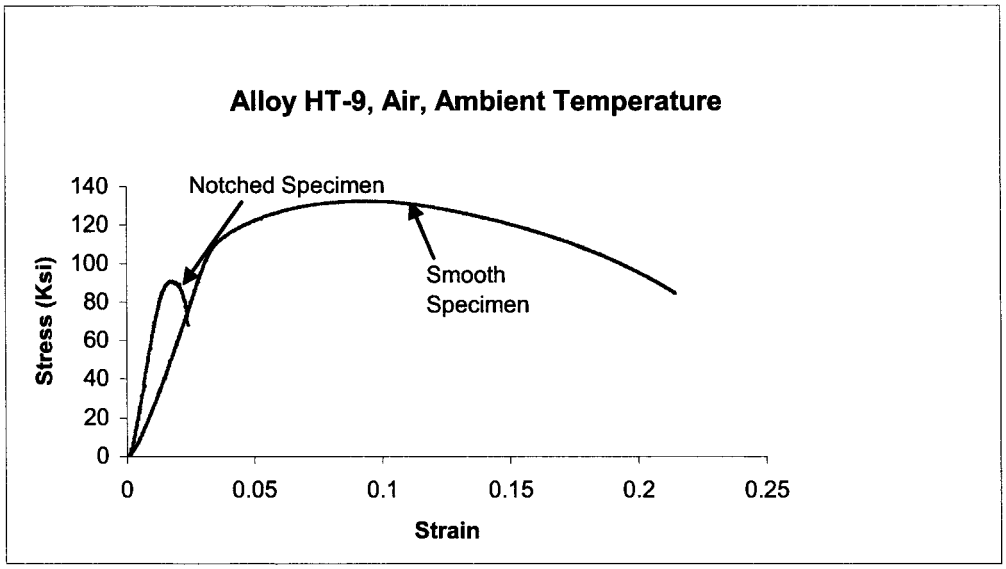

Figure 4.7 Comparison of Stress-Strain Diagram with and without a Notch

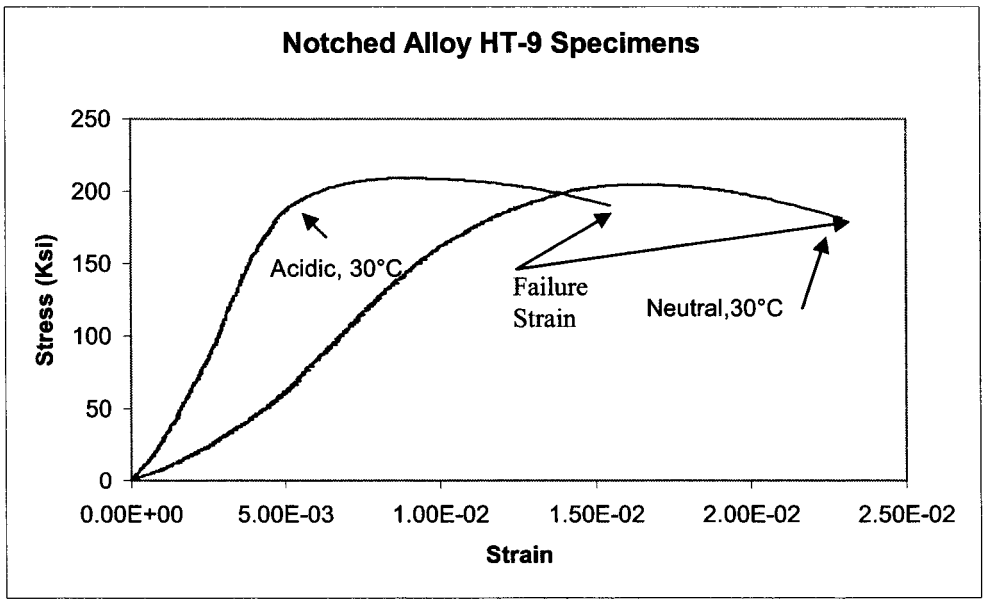

Figure 4.8 Stress-Strain Curves in Neutral and Acidic environments

Table 4.2 SSR Test results using Notched Specimens

Material/ Heat Number/ Heat Treatment/ Specimen ID	Env	Temp (°C)	%El	%RA	UTS (Ksi)	σ_f (Ksi)	TTF (Hour)
HT9/2048/B19	Neutral	30	2.02	22.8	209.79	243.1	4.28
HT9/2048/B22	Neutral	30	1.93	23.99	209.12	250.23	4.3
HT9/2048/B23	Neutral	90	1.67	11.80	177.6	185.01	3.52
HT9/2048/B24	Neutral	90	1.69	12.40	185.27	189.01	3.51
HT9/2048/B27	Acidic	30	1.56	8.16	204.5	201.7	4.2
HT9/2048/B28	Acidic	30	1.53	7.54	200.56	204.03	4.21
HT9/2048/B25	Acidic	90	1.42	6.8	174.051	174.05	3.68
HT9/2048/B26	Acidic	90	1.41	6.8	175.5	173.6	3.52

Temp: Temperature

Env: Environment

%El: Percentage Elongation

%RA: Percentage Reduction in Area

UTS : Ultimate tensile Strength

σ_f : True Failure Stress

TTF: Time-To-Failure

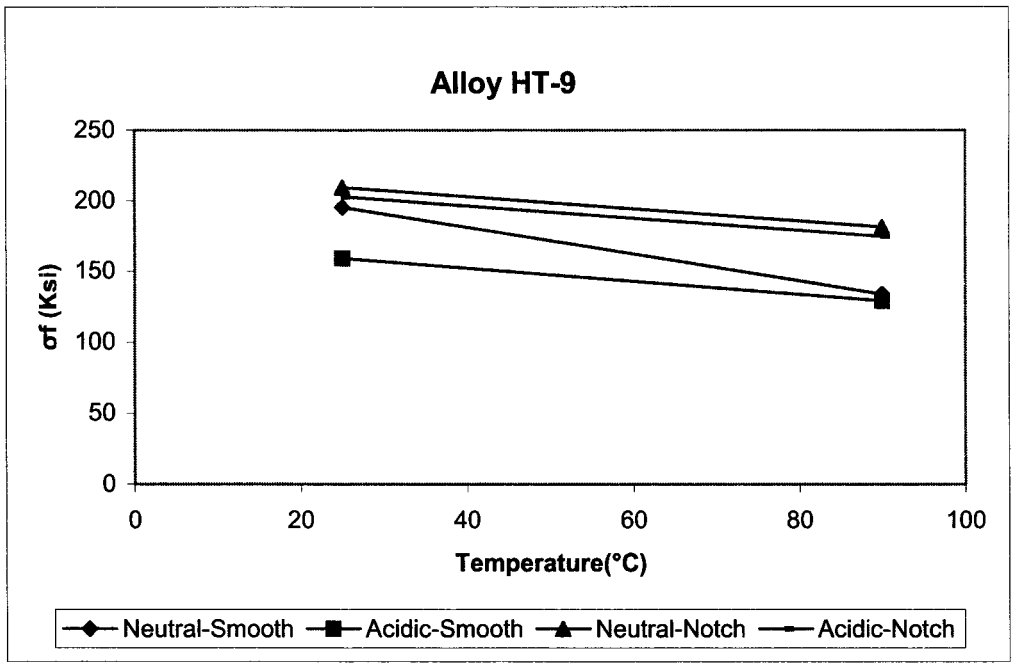

Figure 4.9 Effect of Temperature, pH and Notch on σ_f

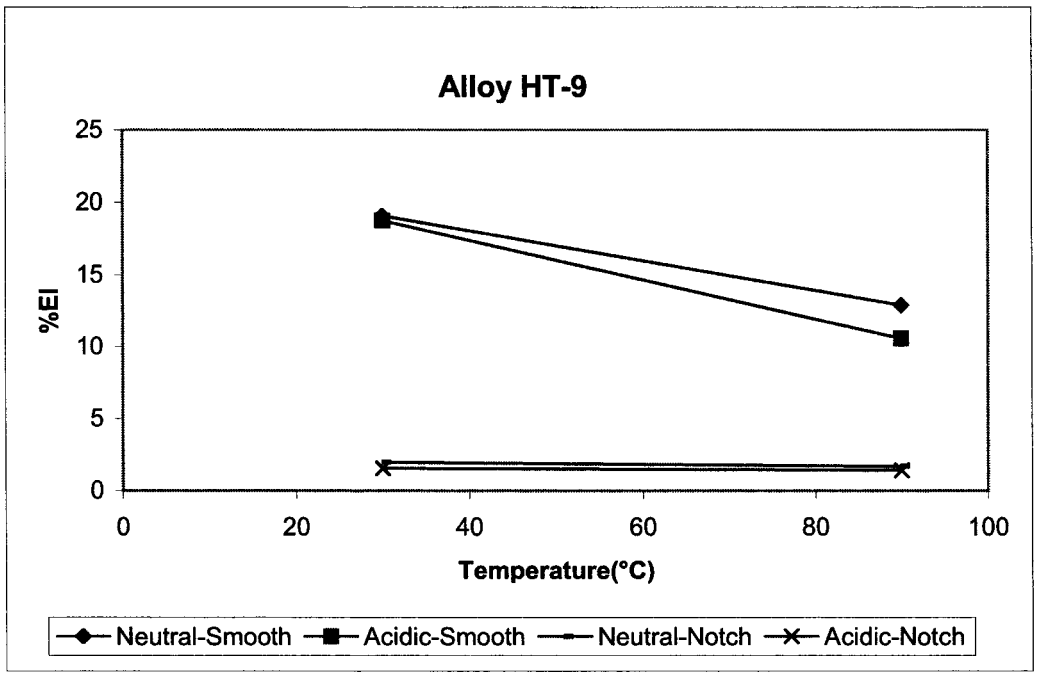

Figure 4.10 Effect of Temperature, pH and Notch on % El

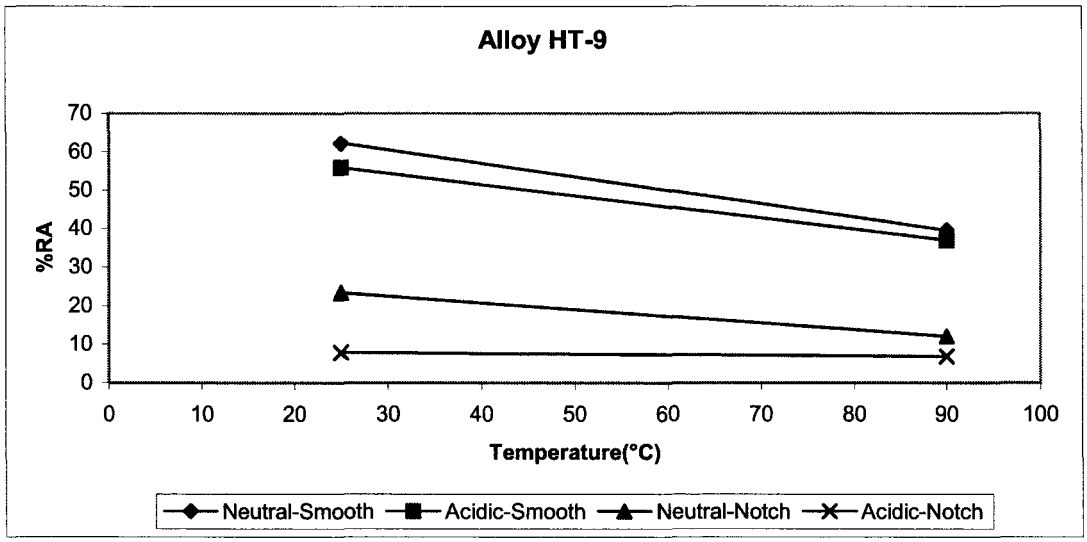

Figure 4.11 Effect of temperature, pH and Notch on % RA

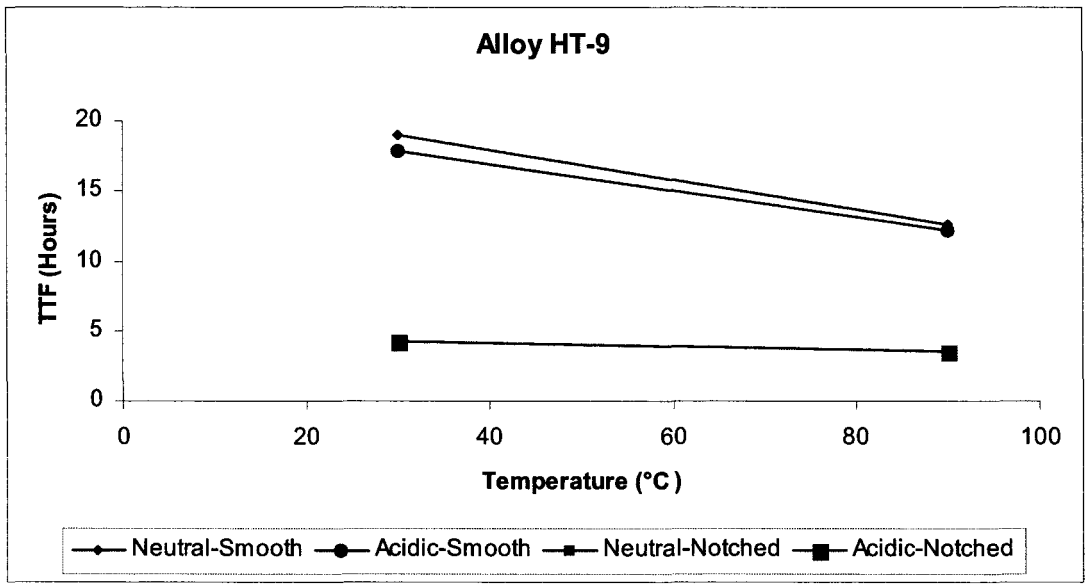

Figure 4.12 Effect of temperature, pH and Notch on TTF

Table 4.3 Comparisons of the Loads with and without a notch

Env	Temp (°C)	Alloy HT-9			
		With notch		Without notch	
		P_m (lb)	P_f (lb)	P_m (lb)	P_f (lb)
Neutral	30	3992	3630	6278	4252
Acidic	30	3858	3466	6250	3554
Neutral	90	3457	3073	5991	3707
Acidic	90	3343	3113	5900	3980

4.1.3. Smooth Specimen with Controlled Potential

SSR tests were performed in the 30 and 90°C acidic solution under a cathodic controlled potential (E_{cont}) of −1000 mV with respect to Ag/AgCl reference electrode. As described earlier, hydrogen can be generated in the aqueous solution during cathodic reaction producing atomic hydrogen (H), which can diffuse at the gage section of the cylindrical specimen and can produce significant amount of stress within the metal lattice. The amount of H generated is related to the magnitude of E_{cont}.

The stress-strain diagrams of Alloy HT-9 in the acidic solution, with and without E_{cont}, at 30 and 90°C are shown in Figures 4.12 and 4.13, respectively. An examination of these figures reveals that the magnitude of UTS and the failure strain was reduced to some extent due to the application of E_{cont} during straining of the test specimen. Table 4.4 shows the comparisons of UTS, %El, %RA, TTF, UTS and σ_f obtained in the acidic solution. These data reveal that the magnitude of all these parameters was reduced during the E_{cont} testing. However, it is interesting to note that the true fracture stress (σ_f) was

reduced to a larger extent due to the applied potential, the effect being more pronounced at 90°C. Nevertheless, these data demonstrate that the presence of hydrogen resulting from potentiostatic cathodic polarization can influence the cracking susceptibility by reducing the ductility, TTF and σ_f, as anticipated.

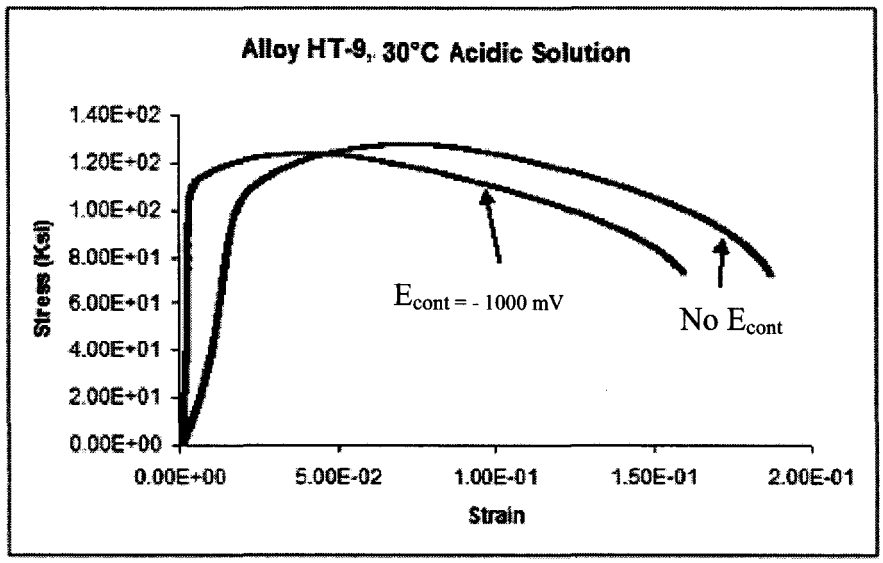

Figure 4.12 Stress-Strain Diagrams with and without E_{cont}

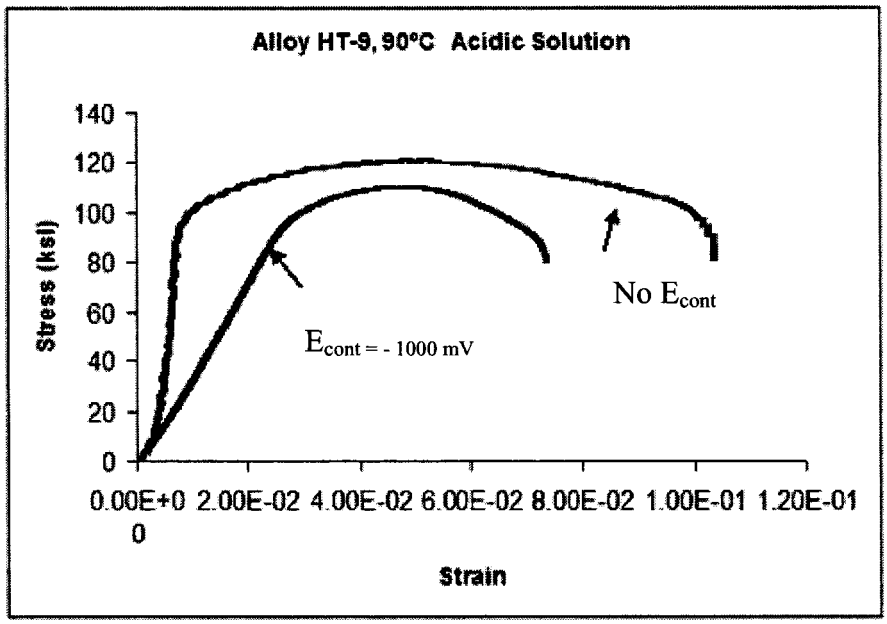

Figure 4.13 Stress-Strain Diagrams with and without E_{cont}

Table 4.4 SSR Test Data for Alloy HT-9 with and without E_{cont}

E_{cont} (mV)	Temp (°C) / Env	%El	%RA	TTF (Hours)	UTS (Ksi)	σ_f (Ksi)
0	30°C/Acidic	19.12	55.96	17.53	128	159
-1000mV	30°C/Acidic	17.32	53.56	12.63	123	138
0	90°C/Acidic	10.58	36.63	11.9	120	115
-1000mV	90°C/Acidic	6.32	28.76	7.89	110	89

Env: Environment Temp: Temperature

4.2. Constant-Load Tests

The results of SCC testing under constant-loading conditions involving smooth and notched cylindrical specimens of Alloy HT-9 are shown in Tables 4.5 and 4.6, respectively. These data indicate that no failures were observed in smooth specimens of this alloy when exposed to the neutral and acidic environments at the ambient temperature even at an applied stress corresponding to the 95 percent (%) of this material's YS value. Failures were observed in the 90°C neutral solution at 0.95YS. Alloy HT-9 exhibited failures in the 90°C acidic solution at applied stresses equivalent to 95, 90, and 85% of its YS value. However, no failures were observed with this alloy at an applied stress corresponding to the 80% of its YS value, suggesting a threshold stress (σ_{th}) of 93 Ksi when tested in 90°C acidic solution, as shown in Figure 4.14. However, the presence of a notch at the gage section of this specimen resulted in a threshold load (L_{th}) of 1084 lbs below which no failure may occur in the acidic solution in the presence of a notch having a diameter of 0.156 inch. It should be noted that all these tests were preformed twice and an average value was considered to get the desired parameters.

Table 4.5 Results of CL SCC Tests using Smooth Specimens

Test No.	Material / Heat No.	Environment Tested		Applied Load		Results
		Temperature (°C)	pH	%YS	Pf (lbs)	TTF
CL-18	HT-9/2048	30	Neutral	95	5588	NF
CL-19	HT-9/2048	30	Neutral	95	5623	NF
CL-14	HT-9/2048	90	Neutral	95	5626	278
CL-15	HT-9/2048	90	Neutral	95	5634	264
CL-16	HT-9/2048	90	Neutral	90	5125	NF
CL-17	HT-9/2048	90	Neutral	90	5189	NF
CL-1	HT-9/2048	30	Acidic	95	5610	NF
CL-2	HT-9/2048	30	Acidic	95	5619	NF
CL-3	HT-9/2048	90	Acidic	95	5668	189
CL-4	HT-9/2048	90	Acidic	95	5653	196
CL-5	HT-9/2048	90	Acidic	90	5185	139
CL-6	HT-9/2048	90	Acidic	90	5130	141
CL-7	HT-9/2048	90	Acidic	85	4834	59
CL-8	HT-9/2048	90	Acidic	85	4820	63
CL-9	HT-9/2048	90	Acidic	85	4740	67
CL-10	HT-9/2048	90	Acidic	80	4444	NF
CL-11	HT-9/2048	90	Acidic	80	4480	NF
CL-12	HT-9/2048	90	Acidic	80	4436	NF

NF: No Failure

Table 4.6 Results of CL SCC Tests using Notched Specimens

Test No.	Material / Heat No.	Environment Tested		Applied Load		Results
		Temperature (°C)	pH	%YL	Pf (lbs)	TTF
CL-1	HT-9/2048	Amb	Acidic	40	1734	NF
CL-2	HT-9/2048	Amb	Acidic	40	1734	NF
CL-3	HT-9/2048	90	Acidic	40	1734	24
CL-4	HT-9/2048	90	Acidic	40	1734	20
CL-5	HT-9/2048	90	Acidic	35	1517	115
CL-6	HT-9/2048	90	Acidic	35	1517	110
CL-7	HT-9/2048	90	Acidic	35	1517	118
CL-8	HT-9/2048	90	Acidic	30	1301	320
CL-9	HT-9/2048	90	Acidic	30	1301	336
CL-10	HT-9/2048	90	Acidic	30	1301	329
CL-11	HT-9/2048	90	Acidic	25	1084	NF
CL-12	HT-9/2048	90	Acidic	25	1084	NF

YL: Yield Load = 4337Psi

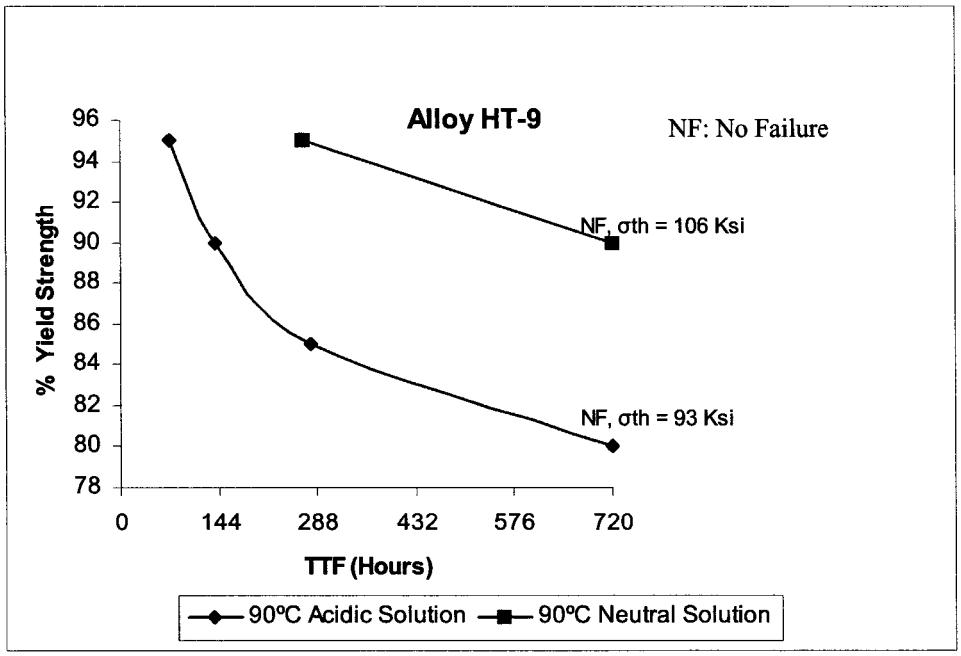

Figure 4.14 Determination of σ_{th} in Neutral and Acidic Environments at 90°C

4.3. Cyclic Potentiodynamic Polarization

The cyclic potentiodynamic polarization (CPP) diagrams for Alloy HT-9 obtained in the acidic solution are shown in Figures 4.15 and 4.16, as a function of the testing temperature. The magnitudes of E_{corr}, E_{pit}, and E_{prot} determined from the CPP diagrams are shown in Table 4.8. An examination of this table clearly indicates that the magnitude of E_{corr} value became more active (negative) in the neutral solution due to a change in temperature from 30 to 60°C. A similar temperature effect on E_{corr} was also observed in the acidic solution, as expected. However, the magnitude of E_{corr} in the acidic solution was more active due to the increased concentration of H^+ in this environment. No pitting was observed in the neutral solution at any tested temperature. However, the test specimens exhibited susceptibility to pitting in the 30 and 60°C acidic solution. As expected, the magnitude of E_{pit} was more active at the higher testing temperature. Protection potentials of -185 and -200 mV (Ag/AgCl) were also observed in the acidic solutions, suggesting repassivation of Alloy HT-9 in these environments.

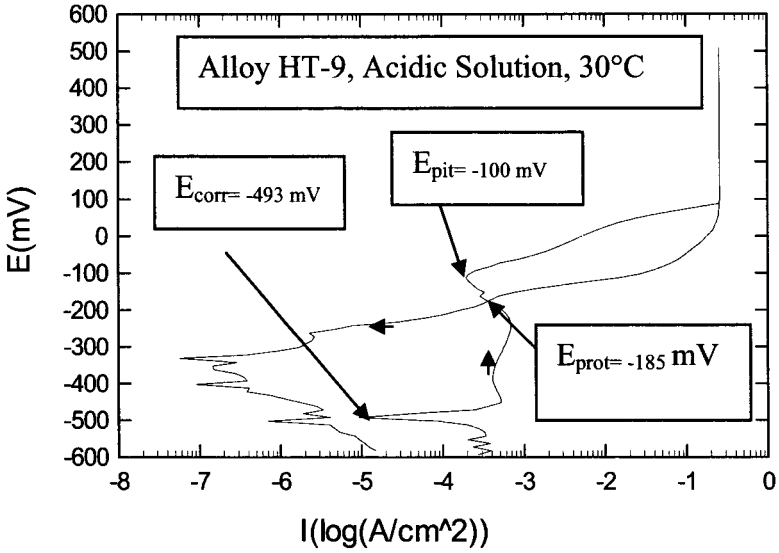

Figure 4.15 CPP Diagram Showing Critical Potentials

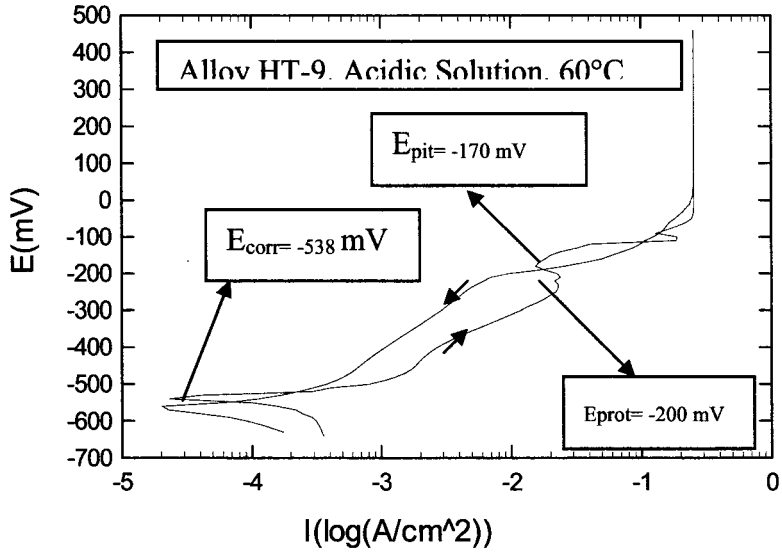

Figure 4.16 CPP Diagram Showing Critical Potentials

Table 4.7 Results of CPP Testing

Material	Env	Temp(°C)	Scan Rate (mV/sec)	E_{corr}, mV (Ag/Agcl)	E_{pit}, mV (Ag/Agcl)	E_{prot}, mV (Ag/Agcl)
Alloy HT-9	Neutral	30	0.166	-185	None	None
		60	0.166	-367	None	None
	Acidic	30	0.166	-493	-100	-185
		60	0.166	-538	-170	-200

4.4. Metallography and Fractography

Efforts were made to investigate the fracture modes of all broken specimens. Based on the fractographic evaluations, it appears that the primary failure mode at the gage section of specimens tested in the 90°C neutral solution was ductile, showing dimpled microstructures (Figure 4.17), irrespective of loading condition. On the contrary, the specimens tested in the 90°C acidic solution showed intergranular and/or transgranular brittle failures, as shown in Figure 4.18 for both constant load and SSR testing. Elemental analysis in the vicinity of the cracks, performed by the energy dispersive spectrometry (EDS) primarily showed significant concentrations of Fe and Cr, as illustrated in Figure 4.19. Other alloying elements present in Alloy HT-9 were also noticed.

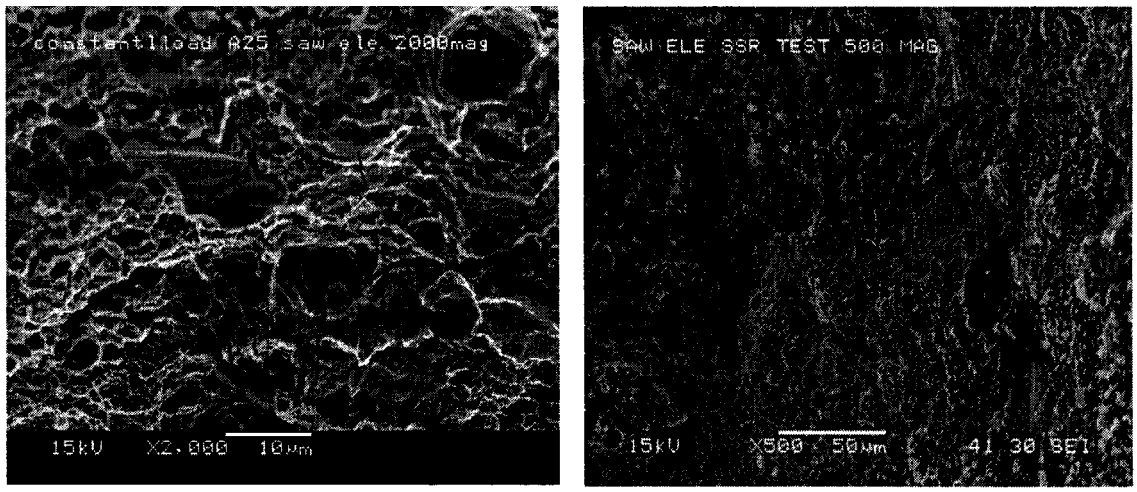

(a) Constant Load Test (b) SSR Test

Figure 4.17 SEM Micrographs of Alloy HT-9 at 90°C in Neural Environment

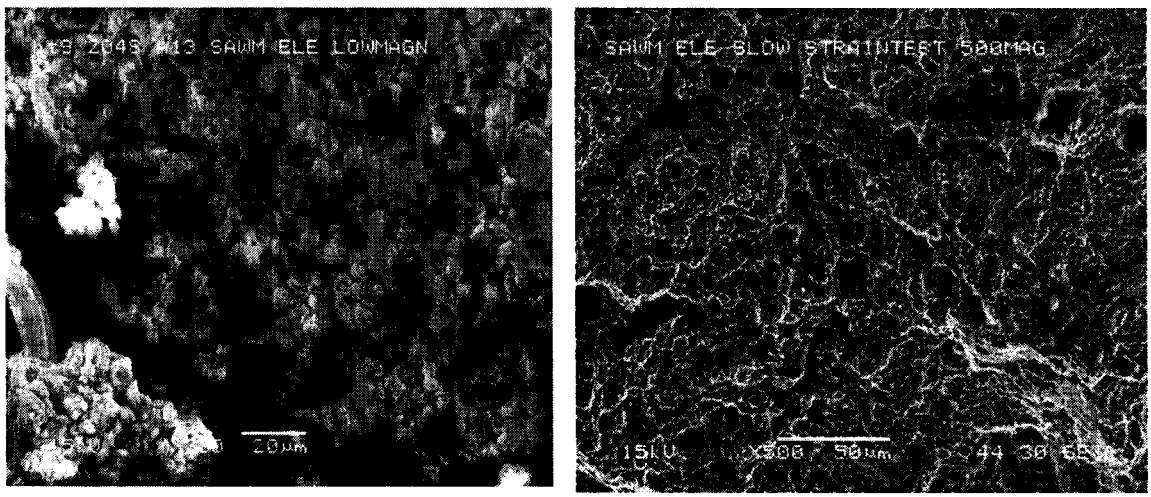

(a) Constant Load Test (b) SSR Test

Figure 4.18 SEM Micrographs of Alloy HT-9 in 90°C Acidic Environment

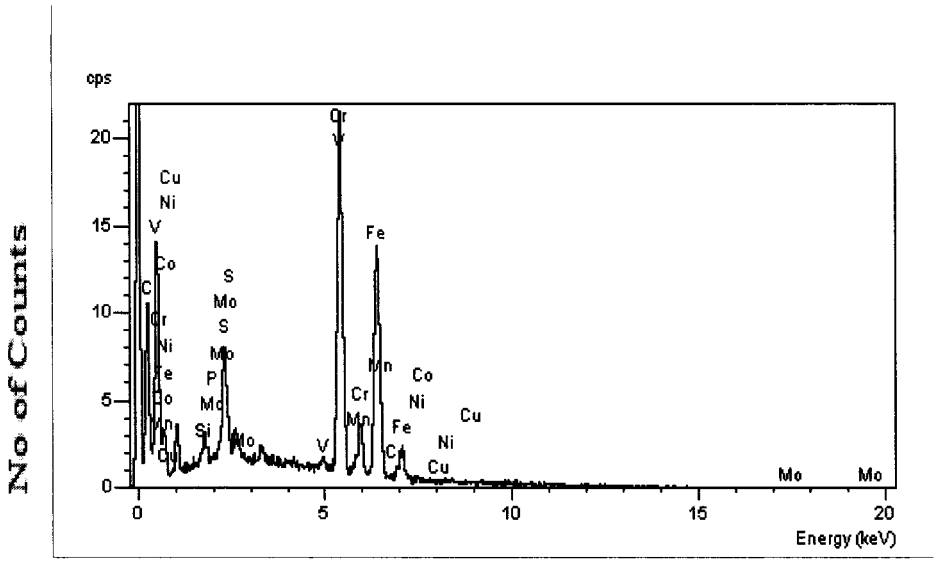

Figure 4.19 Elemental Analyses by EDS

The metallographic evaluation of the gage section of the broken specimen by optical microscopy revealed branched secondary cracks, as shown in Figure 4.20

Figure 4.20 Alloy HT-9 Showing Secondary Cracks, (50X)

CHAPTER 5

DISCUSSION

As described earlier, this investigation is aimed at evaluating environment-induced degradations including SCC, HE and localized corrosion behavior of a target structural material, namely Alloy HT-9 in molten LBE. Since experimental work involving the molten LBE environment could not be accommodated at UNLV, an effort was made to perform the LBE testing at LANL. Simultaneously, an extensive experimental program was pursued at the Materials Performance laboratory (MPL) at UNLV to develop baseline corrosion data on the susceptibility of Alloy HT-9 to SCC, HE and localized corrosion (pitting and crevice) in aqueous environments at ambient and elevated temperatures using different state-of-the-art testing techniques. A brief, but relevant discussion of the resultant data using different experimental methods is presented below.

5.1. SCC – Constant-Load Testing

The results of constant-load SCC testing in a 90°C neutral solution using smooth tensile specimens of Alloy HT-9, shown in the previous section, indicate that this material may undergo failure at an applied stress level corresponding to 95% of its YS value. However, failures have been observed in the 90°C acidic solution when tested at applied stresses equivalent to 95, 90 and 85% of this material's YS value. Since no

failures were observed at 0.80YS in this environment, a threshold stress (σ_{th}) in the vicinity of 93 Ksi was established for this alloy in this environment. A synergistic effect of pH and temperature can be attributed to this observed reduction in σ_{th} in the 90°C acidic solution. It should, however, be noted that the presence of a stress raiser (notch) in the smooth specimen reduced the threshold load (L_{th}) to 25% of its yielding load (notched specimen) in the similar environment at 90°C. Based on these results, a threshold load (L_{th}) of 25-30% of the yielding load can be suggested for the notch configuration used in this study. A similar effect of notch on the cracking susceptibility of engineering alloys has been demonstrated by other investigators [19].

5.2. SCC – SSR Testing

The results of SCC testing performed under a SSR condition using both smooth and notched specimens indicates that the ductility parameters (%El and %RA) and TTF were reduced with increasing temperature, irrespective of the solution pH. The temperature effects on these parameters are consistent with observation made by other investigators [20, 21]. Once again, the presence of a notch at the gage section of the test specimen resulted in significant reduction in all these parameters, as expected. The only exception to these results was with the effect of notch on the true failure stress (σ_f) that was enhanced due to the reduced cross sectional area at the root of the notch.

5.3. SCC - E_{cont} Testing

It is well known that an electrochemical reaction consists of anodic and cathodic reactions. The anodic or oxidation reaction produces a metal ion (M^+) and an electron, which is used in the reduction of hydrogen ion (H^+) to produce atomic hydrogen (H). During potenstiostatic polarization in an acidic solution under cathodic control, more H^+ ion can be generated causing increased concentration of H that can diffuse into the metal lattice within a certain temperature regime. This phenomenon is known as HE. While many theories exist on HE, it is known that the presence of H can weaken the cohesive bond of the surface film existing in materials of interest. As expected, the magnitude of the failure strain was reduced with the change in temperature from 30 to 60°C. This effect was more pronounced when an external potential of -1000mV (Ag/AgCl) was potenstiostatically applied to the tensile specimen, as shown in Figures 4.12 and 4.13. Simultaneously, the magnitude of σ_f was reduced to some extent due to these changes in environmental conditions, as expected [22].

5.4. Localized Corrosion - CPP Testing

The results of CPP testing of Alloy HT-9 showed more active E_{corr}, E_{pit} and E_{prot} values in the acidic solution compared to that in the neutral environment. Simultaneously relatively more active E_{corr}, E_{pit} and E_{prot} values were observed at higher testing temperatures, as expected. Electrochemically speaking, more active (negative) potential is a characteristic of enhanced localized corrosion susceptibility. These active (negative) potentials may be attributed to more acidic pH and higher testing temperature. A similar phenomenon has been reported by the other investigators [23].

5.5. Fractography and Metallography

Fractographic evaluations by SEM revealed dimpled microstructure in Alloy HT-9 when tested in the neutral solution, indicating a ductile failure. On the contrary, brittle failures were characterized by intergranular and/or transgranular cracking in the acidic solution, irrespective of the testing temperature. Branched secondary cracks were also observed along the gage section of the tested specimens, determined by optical microscopy.

CHAPTER 6

SUMMARY AND CONCLUSIONS

The susceptibility of Alloy HT-9 to SCC, HE and localized corrosion has been evaluated in aqueous environments of different pH values at ambient and elevated temperatures. For SCC testing, both constant load and SSR techniques have been used. The susceptibility to HE has been determined by cathodic charging of the cylindrical specimens. CPP tests have been performed to evaluate the localized corrosion behavior of test material. SEM and optical microscopy have been used for failure analysis and microstructural evaluation, respectively. The significant conclusions derived from this study are given below.

- Alloy HT-9 showed failures in the 90°C acidic solution under constant loading at applied stresses of 95, 90 and 85% of its YS value. No failures, however, were observed at 80% of its YS, resulting in a σ_{th} value of 93 ksi.
- Constant load SCC testing in the 90°C Neutral solution showed failure in Alloy HT-9.
- The magnitudes of ductility parameters and TTF were gradually reduced in both tested environments with increasing temperature. The presence of a notch further reduced these parameters. However, magnitude of σ_f was increased due to a smaller cross sectional area at the root of this notch.

- The application of a cathodic potential to the test specimens showed a detrimental effect of H in enhancing its cracking susceptibility in an acidic environment.
- The specimens, polarized in the acidic solution, were characterized by pits and crevices. The pitting susceptibility was enhanced at 60^{o} showing more active E_{corr}, E_{pit}, and E_{prot} values. No localized attack was observed in the neutral solution.
- Secondary cracks with branching were detected at the gage section of the failed specimen, by metallographic technique.

FUTURE WORK

- Assuming that a research facility to accommodate molten LBE testing is established at UNLV, SCC testing needs to be conducted in this environment at temperatures ranging from 400 to 550°C, using self-loaded (C-ring and U-bent) specimens. Efforts may also be made to see if localized dissolution of the surface film may occur in this temperature regime.
- Characterize the surface film in Alloy HT-9 specimens tested in aqueous and molten LBE environments at comparable temperatures using relevant testing techniques.

APPENDIX A

LOAD VS DISPLACMENT PLOTS FOR SMOOTH SPECIMENS

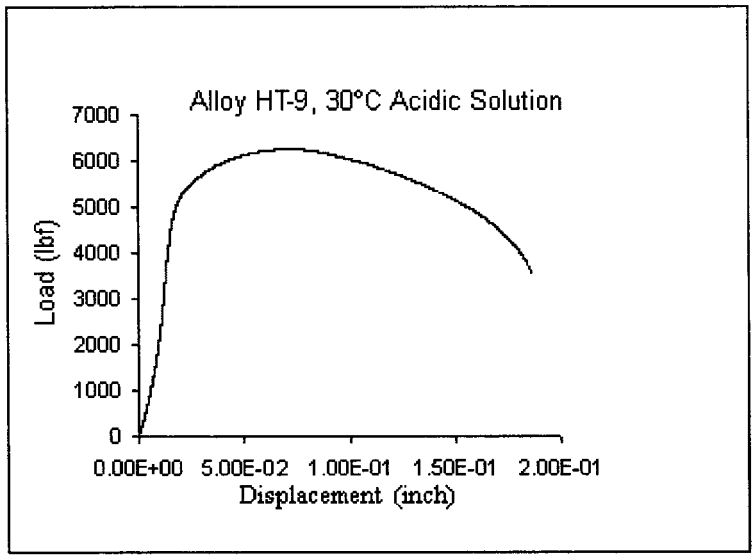

Alloy HT-9 in 30°C Acidic Solution (Sample-1)

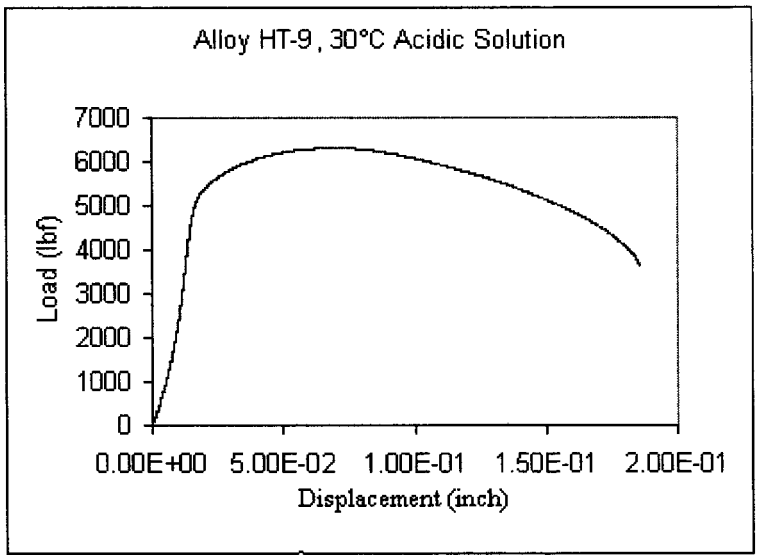

Alloy HT-9 in 30°C Acidic Solution (Sample-2)

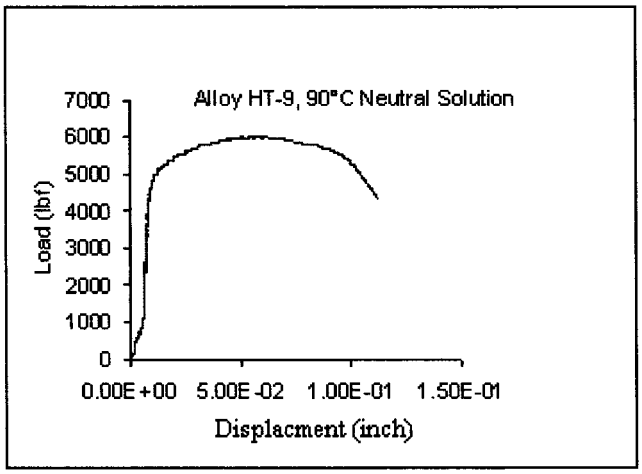

Alloy HT-9 in 90°C Neutral Solution (sample-1)

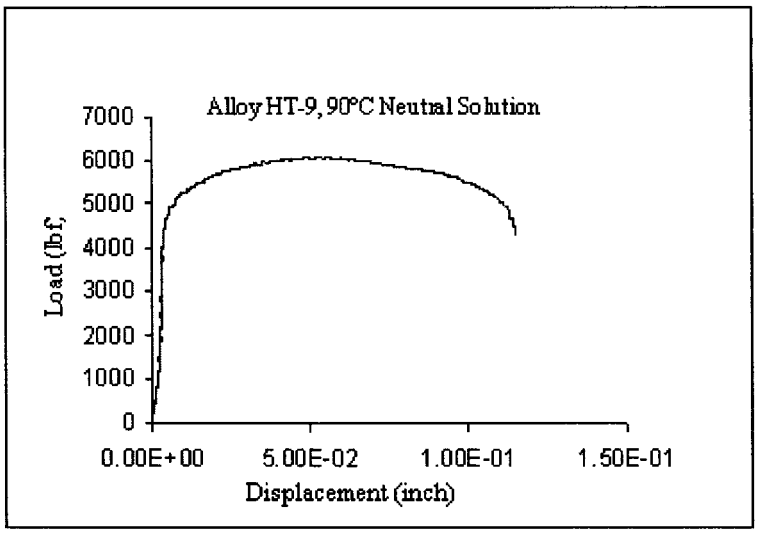

Alloy HT-9 in 90°C Neutral Solution (sample-2)

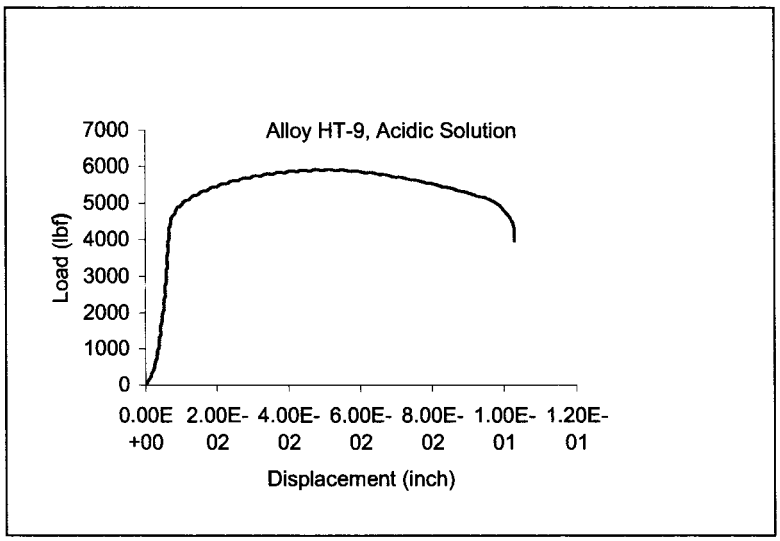

Alloy HT-9 in 90°C Acidic Solution (Sample-1)

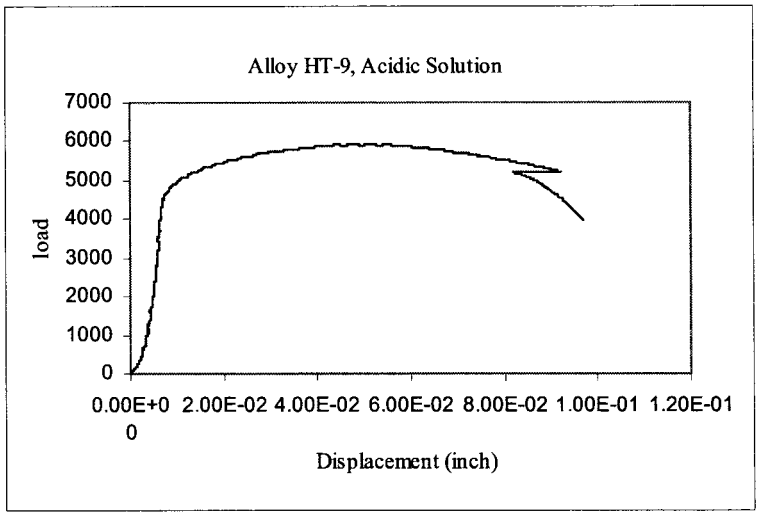

Alloy HT-9 in 90°C Acidic Solution (Sample-2)

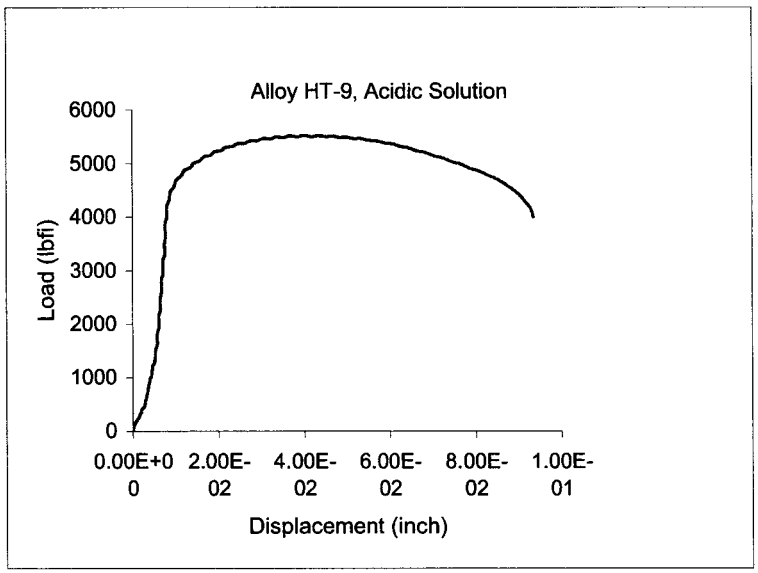

Alloy HT-9 in 90°C Acidic Solution (Sample-3)

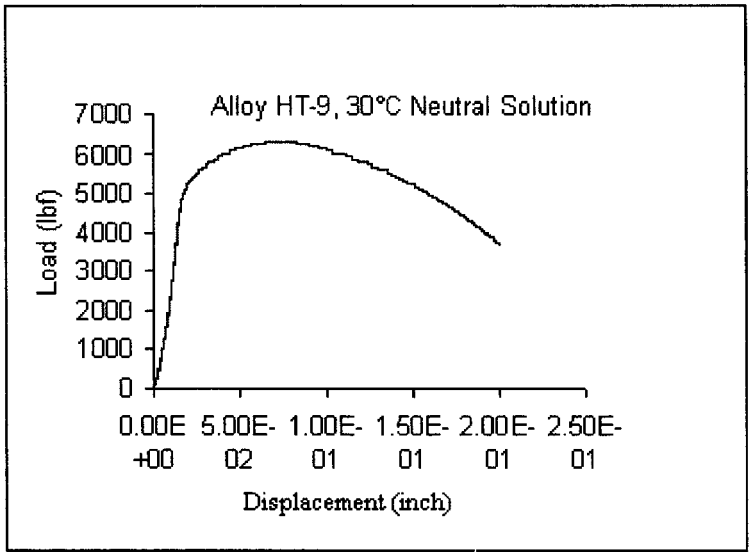

Alloy HT-9 in 30°C Neutral Solution (Sample-1)

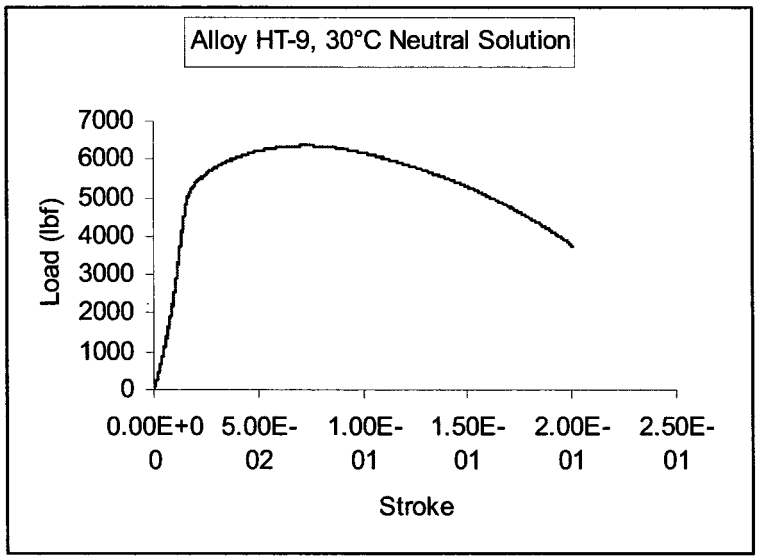

Alloy HT-9 in 30°C Neutral Solution (Sample-2)

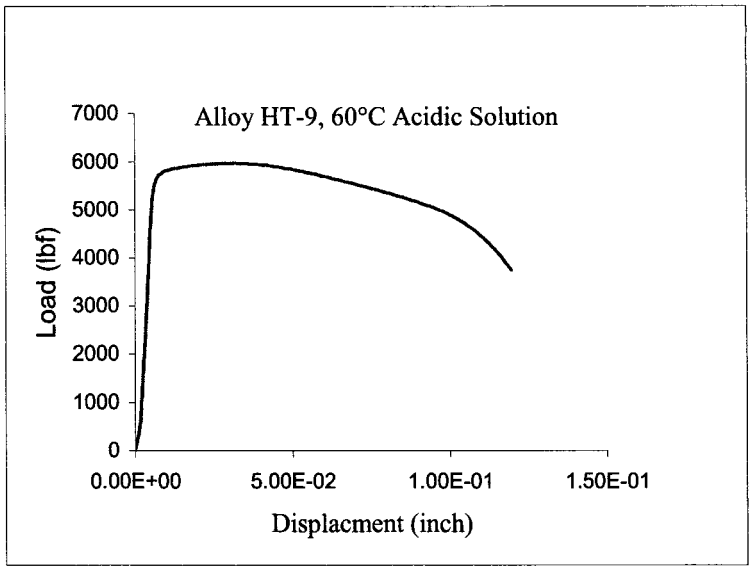

Alloy HT-9 in 60°C Acidic Solution (Sample-1)

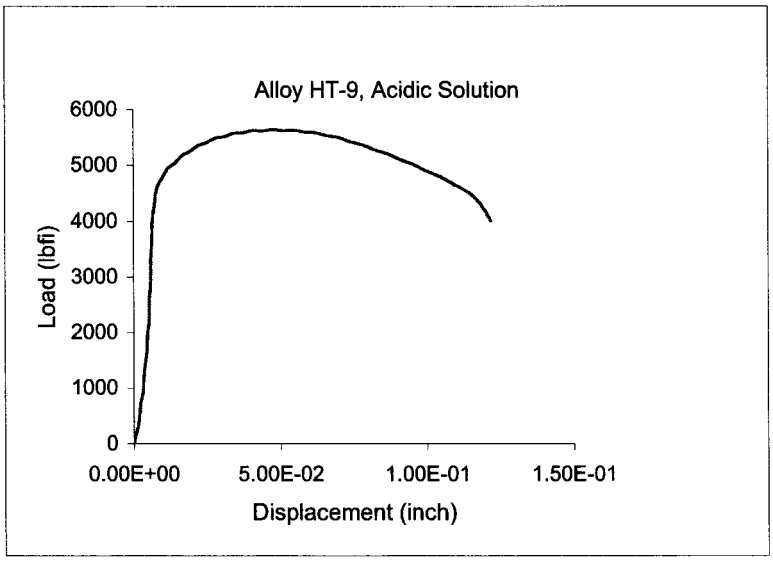

Alloy HT-9 in 60°C Acidic Solution (Sample-2)

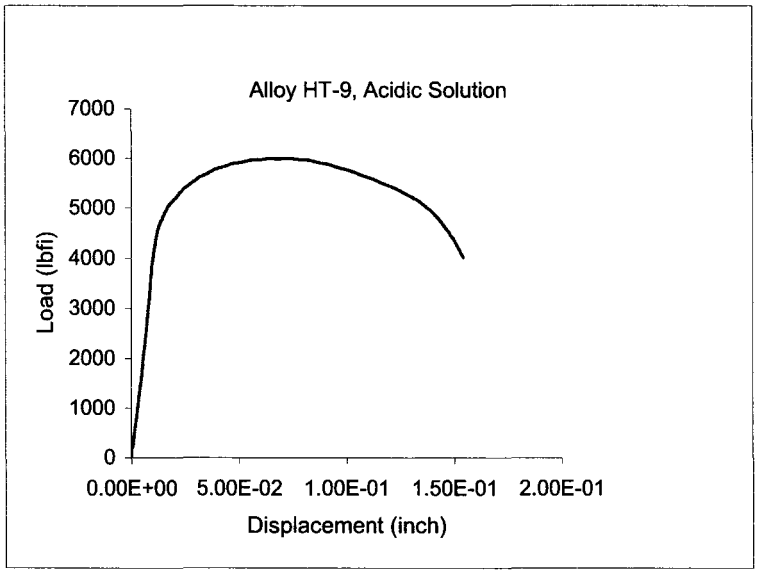

Alloy HT-9 in 60°C Acidic Solution (Sample-3)

APPENDIX B

LOAD VS DISPLACEMENT PLOTS FOR NOTCHED SPECIMENS

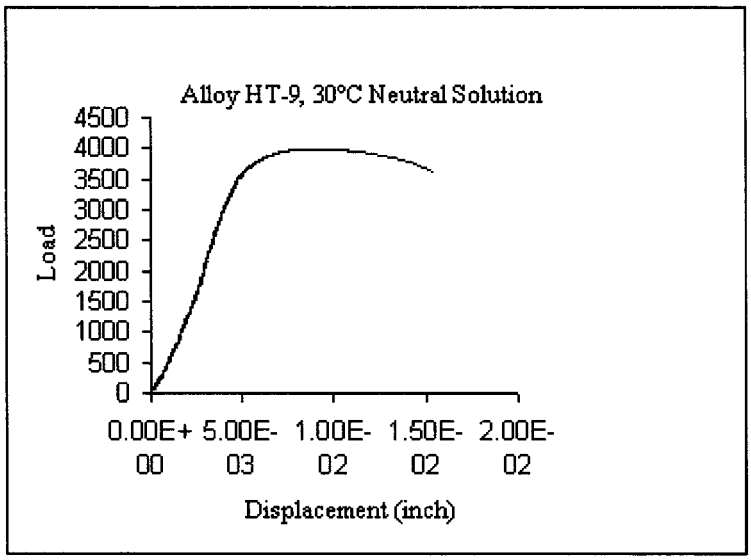

Alloy HT-9 in 30°C Neutral Solution (Sample-1)

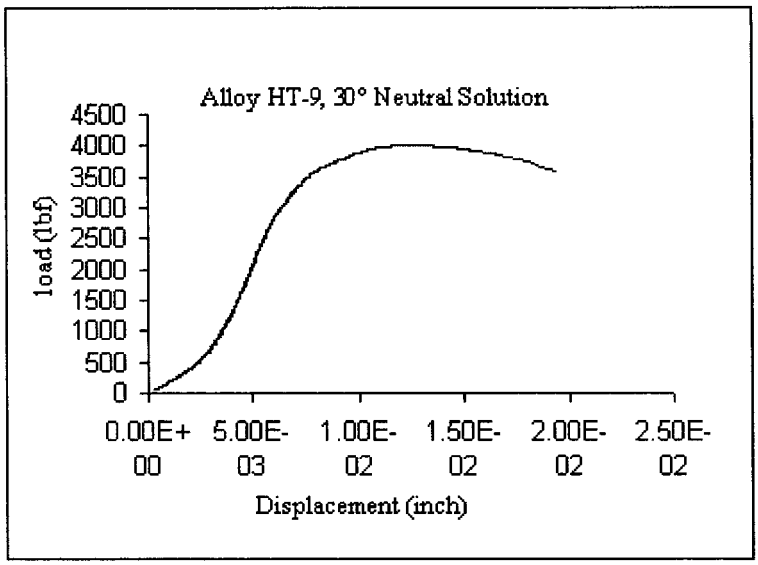

Alloy HT-9 in 30°C Neutral Solution (Sample-2)

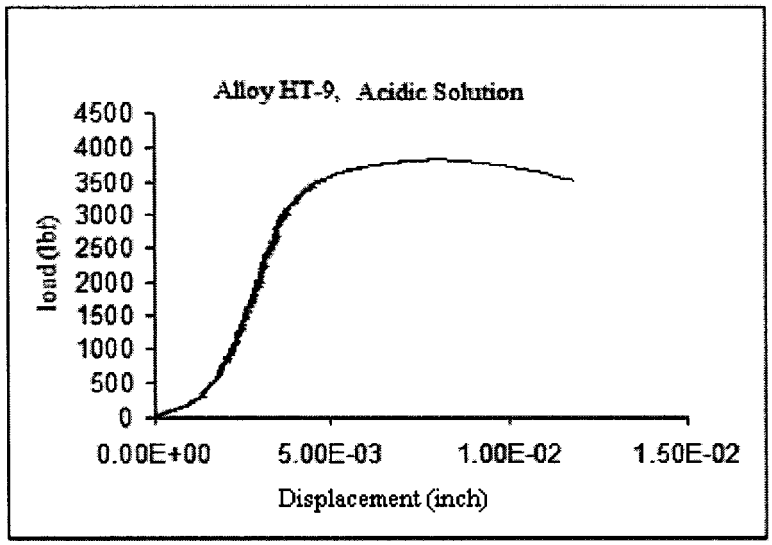

Alloy HT-9 in 30°C Acidic Solution (Sample-1)

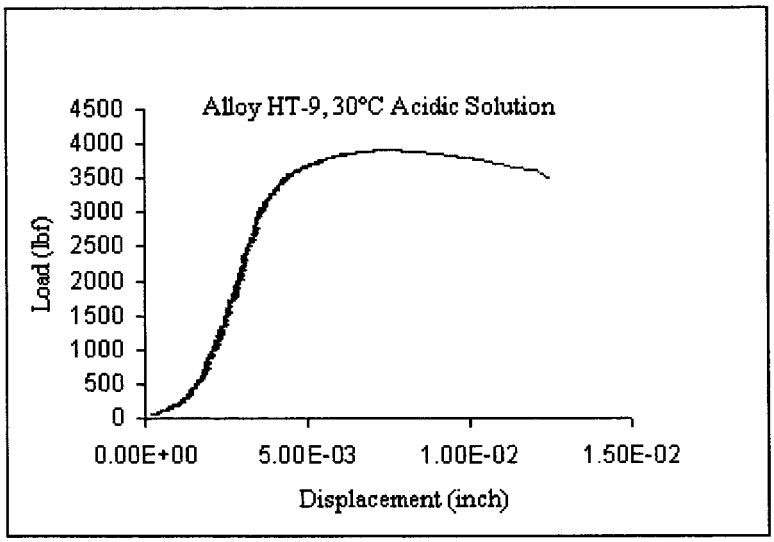

Alloy HT-9 in 30˚C Acidic Solution (sample-2)

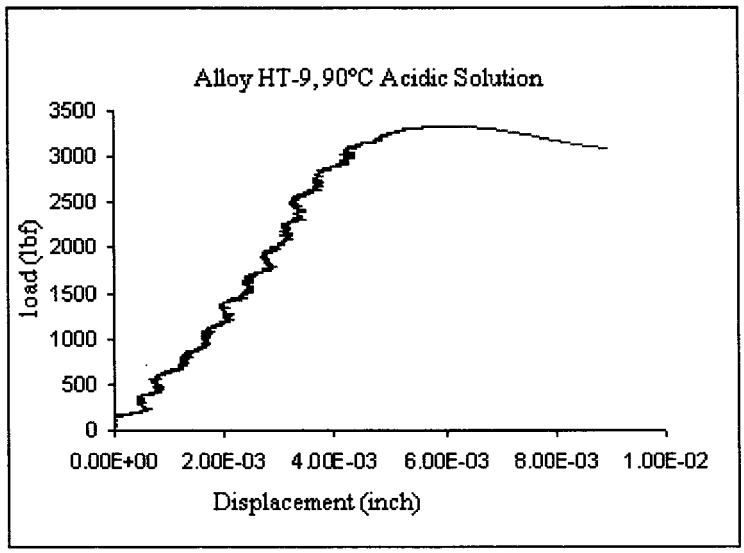

Alloy HT-9 in 90˚C Acidic Solution (Sample-2)

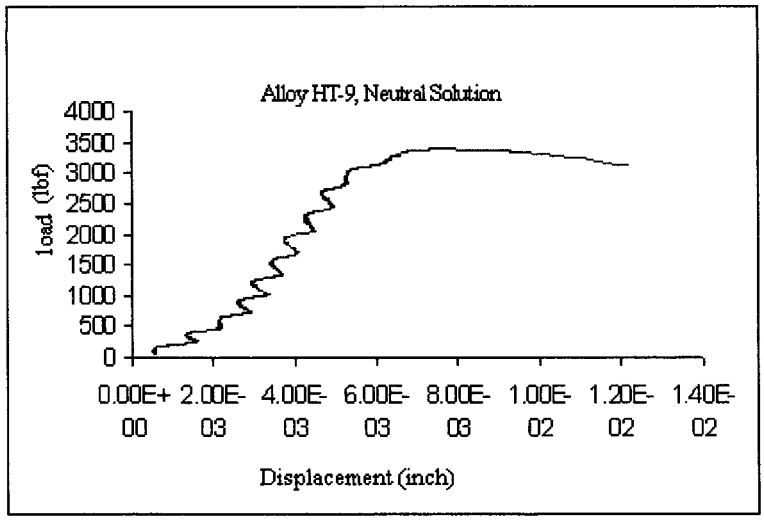

Alloy HT-9 in 90°C Neutral Solution (Sample-1)

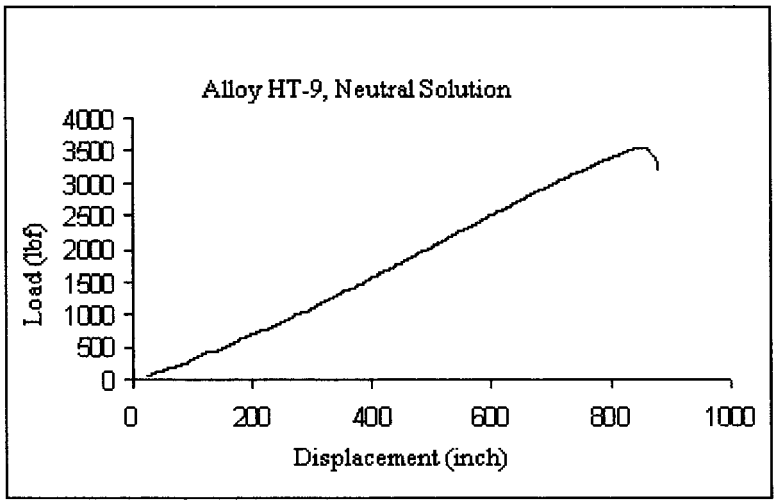

Alloy HT-9 in 90°C Neutral Solution (Sample-2)

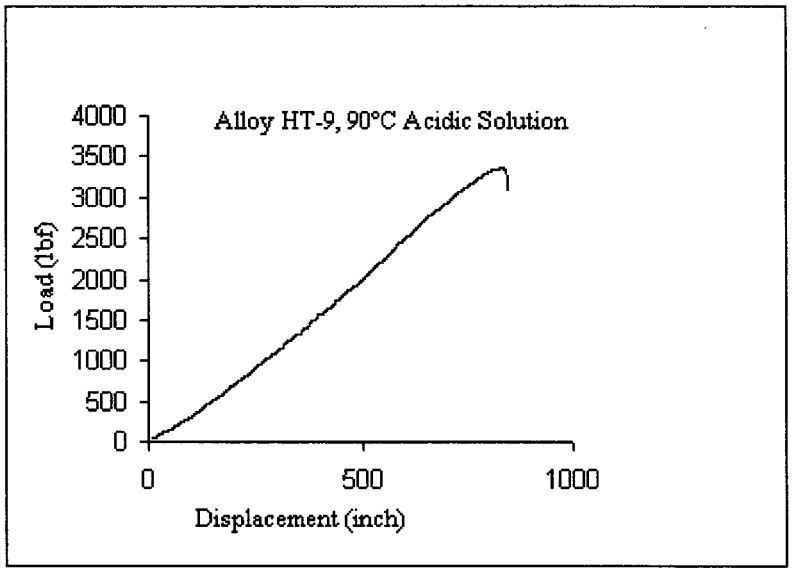

Alloy HT-9 in 90˚ Acidic Solution (Sample-2)

APPENDIX C

LOAD VS DISPLACEMENT PLOTS UNDER E_{CONT} IN ACIDIC SOLUTION

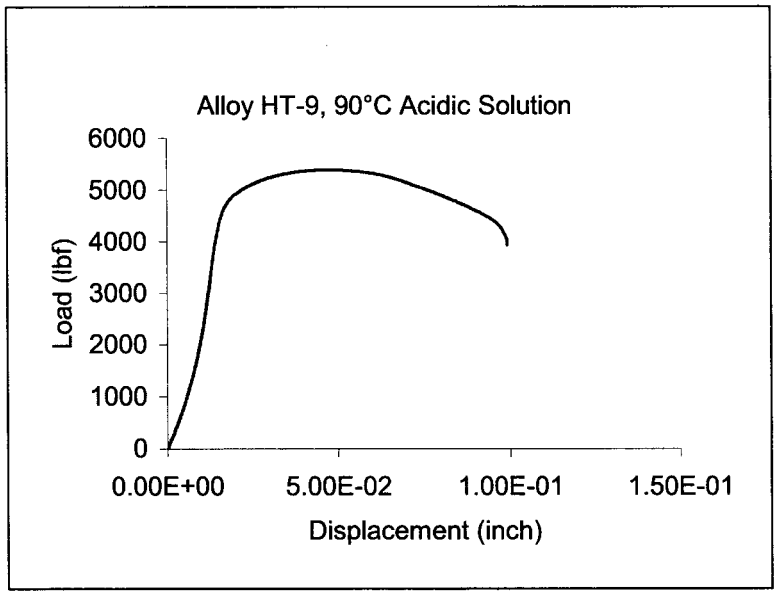

Alloy HT-9 in 90°C Acidic Solution under E_{cont} = -1000mV

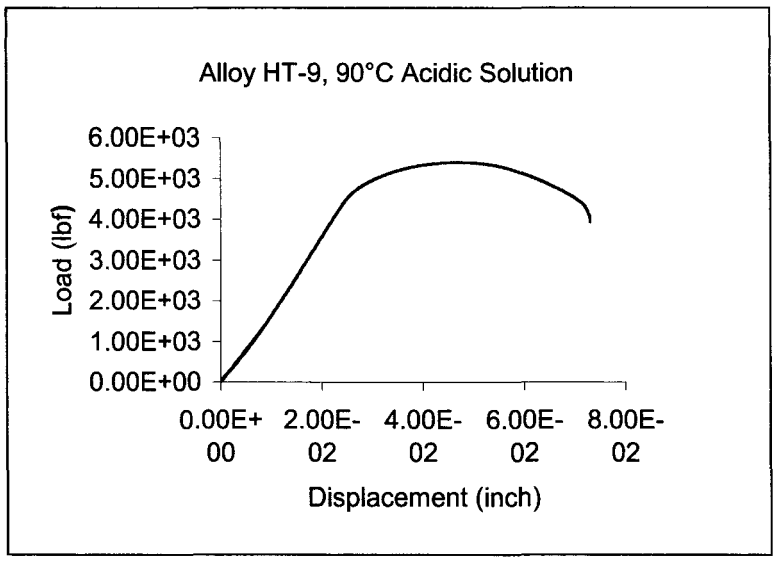

Alloy HT-9 in 90°C Acidic Solution under E_{cont} = -1000mV

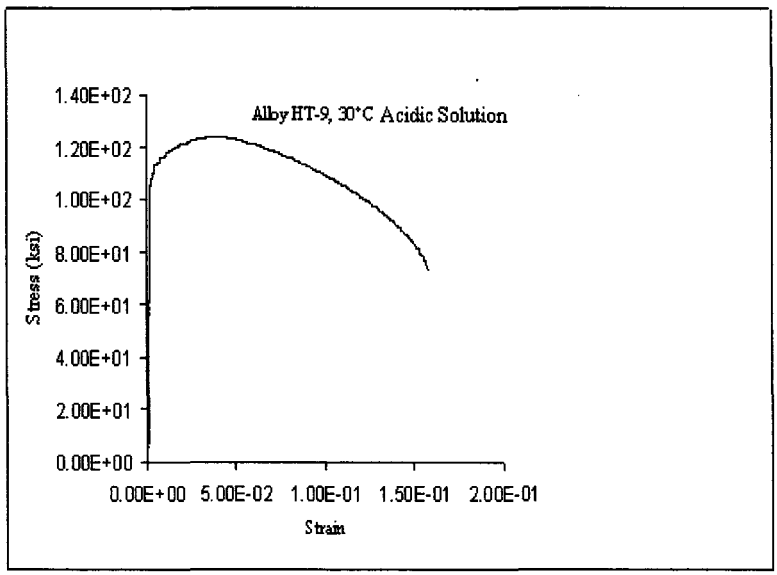

Alloy HT-9 in 30°C Acidic Solution under E_{cont} = -1000mV

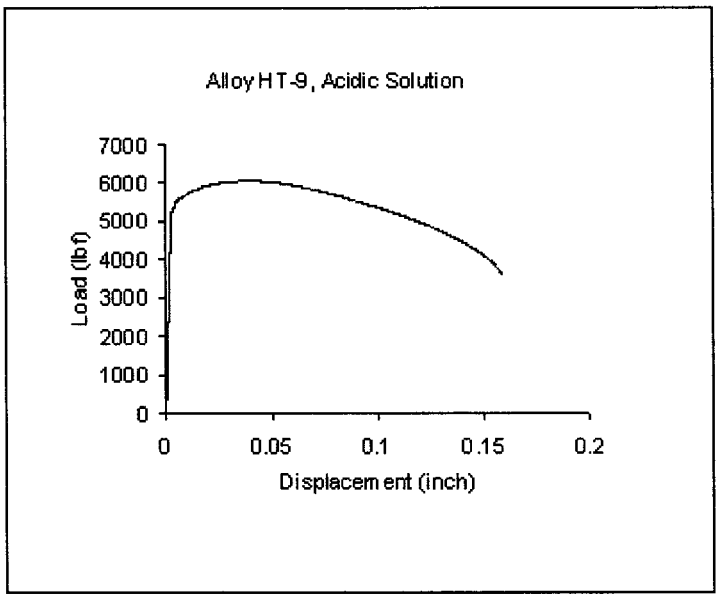

Alloy HT-9 in 30°C Acidic Solution

BIBILOGRAPHY

1 www.lanl.gov/transmutation

2 Mikhail Kh khankhasayev, Zhanat B kurmanov and Hans S Plendl., Nuclear Methods for Transmutation of Nuclear Waste, 1996, p. 5-10

3 www.lanl.gov/ lead-bismuth Eutectic

4 George E. Dieter., Mechanical Metallurgy, 1998, p. 496-500

5 Mars G. Fontana., Corrosion Engineering, 1987, p. 137-152

6 Nelson HG. Hydrogen embrittlement. In: Briant CL, Banerji SK, editors. Treatise on materials science and technology, vol. 25. New York: Academic Press, 1983. p. 275-359.

7 D. H Mesa, A. Toro, A. Sinatora, A.P Tschiptschin, The Effect of testing temperature on corrosion-erosion resistance of martensitic stainless steels.

8 H.E Boyer (Ed.), Metals Handbook, vol. 10, American Society for Metals, Metals Park, Ohio, 1975, pp. 217-218.

9 Kimura, A. and H. Matsui, "Neutron Irradiation Effects on the Microstructure of Low-Activation Ferritic Alloys, "J. Nucl. Mater. 212-w215, 1994,701.

10 Lucas , G.e., Odette, G.R., Maiti, R., Sheckherd, J. w., "Tensile Properties of irradiated Pressure Vessel Steels," ASTM-STP-956, American Society for Testing and Materials, 1987, p379-385

11 Elliott, C., Lucas, G.E., Maiti, R., Odette, G.R., "Microstructure of HT-9 as a function of Heat Treatment," J.Nucl.Mater., 141-143, 1986, p794

12 http://www.uwisc.edu

13 A.J. GRIFFITHS and A.TURNBULL: Proc. Conf on Structural Materials in Marine Environments', London, UK, May 1994, the Institute of Materials, 324-329.

14 March, J.L., Ruprecht, W. J., and Reed, George, "Machining of Notched Tension Specimens," ASTM Bulletin, ASTBA, Am.Soc.Testing Mats., No.244 1960, pp.52-55

15 ASTM Designation: E 8-89b, Standard Test Methods of Tension Testing of Metallic materials

16 ASTM Designation: G61-78, Standard Practice for Conducting Cyclic Potentiodynamic Polarization Measurements for Localized corrosion.

17 http://www.cortest.com

18 A. K. Roy, et al., "Cracking of Titanium Alloys under Cathodic Applied Potential," Micron, Vol. 32, No. 2, Elsevier Science, February 2001, pp. 211-218

19 N.Eliaz, A.Shachar, B.tal, D.Elizier, Characteristics of hydrogen embrittlement, stress corrosion cracking and tempered martensite embrittlement in high-strength steels, December 2000

20 Jones RH, Ricker RE. Stress-Corrosive Cracking. In: Metals handbook, vol.13. 9th ed. Ohio: ASM International, 1987.p.145-63

21 Hertzberg RW. Deformation and fracture mechanics of engineering materials. 4th ed. Newyork: John wiley & Sons, 1996. P.460-4: 485-520.

22 Birnbaum HK. Mechanisms of hydrogen related fracture of metals. In: Moody NR, Thompson AW, editors. Proceedings of the fourth International Conference on the effect of Hydrogen on the behavior of Materials. Wyoming, 1990: Warrandale: TMS,

1989. p. 639-60.

23 D.H. Mesa, A.Toro, A.Sinatora, A.P. Tschiptschin, The effect of testing temperature on corrosion-erosion resistance of martensitic stainless steels.

VITA

Graduate College
University of Nevada, Las Vegas
Sudheer Sama

Local Address:
1170 Maryland Circle Apt. #1
Las Vegas, NV 89119

Degrees:
Bachelors of Science, Mechanical Engineering, 2000
Gulbarga University, India

Thesis Title: Embrittlement and Localized Corrosion in Alloy HT-9

Thesis Examination Committee:
Chairperson, Dr. Ajit K. Roy, Ph. D.
Committee Member, Dr. Brendan. J. O'Toole, Ph. D.
Committee Member, Dr. Anthony E. Hechanova, Ph. D.
Graduate Faculty Representative, Dr. Satish Bhatnagar, Ph. D.